

Research Article

Late Paleozoic–Early Mesozoic granitoids in the Khangay-Khentey basin, Central Mongolia: Implication for the tectonic evolution of the Mongol-Okhotsk Ocean margin

Ariuntsetseg Ganbat^{a,b,*}, Tatsuki Tsujimori^{a,c}, Laicheng Miao^d, Inna Safonova^{e,f}, Daniel Pastor-Galán^{a,c,g}, Chimedtseren Anaad^{b,i}, Munkhtsengel Baatar^{b,h}, Shogo Aoki^{j,k}, Kazumasa Aoki^k, Ilya Savinskiy^e

^a Department of Earth Science, Graduate School of Science, Tohoku University, Aoba, Sendai 980-8578, Japan

^b Geoscience Center, Mongolian University of Science and Technology, Ulaanbaatar 120646, Mongolia

^c Center for Northeast Asian Studies, Tohoku University, Aoba, Sendai 980-8576, Japan

^d Institute of Geology and Geophysics, Chinese Academy of Sciences, Beijing 100029, China

^e Novosibirsk State University, Pirogova St. 1, Novosibirsk 630090, Russia

^f Sobolev Institute of Geology and Mineralogy, SB RAS, Koptyuga ave. 3, Novosibirsk 630090, Russia

^g Frontier Research Institute for Interdisciplinary Sciences, Tohoku University, Aoba, Sendai 980-0845, Japan

^h Mongolian University of Science and Technology, Ulaanbaatar 120646, Mongolia

ⁱ Natural History Museum of Mongolia, Ulaanbaatar 120646, Mongolia

^j Graduate School of International Resource Sciences, Akita University, Akita 010-8502, Japan

^k Center for Fundamental Education, Okayama University of Science, Okayama 700-0005, Japan

ARTICLE INFO

Keywords:

CAOB
Mongol-Okhotsk Ocean
Geochronology
Crustal evolution
Hf-in-zircon
Nd isotope

ABSTRACT

The Mongol-Okhotsk Belt is the youngest segment of the Central Asian Orogenic Belt, which is the venue of the massive juvenile crust emplacement, and its formation and evolutions are still pending problems. This paper presents the first up-to-date U–Pb zircon ages, Hf-in-zircon isotope, geochemical and whole-rock Nd isotope data from igneous rocks of the Khangay-Khentey basin, Central Mongolia. The U–Pb zircon ages indicate three groups of magmatism at ~296 Ma, ~280 Ma, and ~230 Ma. The ~296 Ma magmatic rocks are characterized by negative $\varepsilon_{\text{Hf}}(t)$ and $\varepsilon_{\text{Nd}}(t)$ values and old Hf and Nd model ages suggesting their derivation by the melting of the crustal source. The ~280 Ma rocks are A_2 -type monzonites, granitoids, and rhyolites show positive $\varepsilon_{\text{Hf}}(t)$ and $\varepsilon_{\text{Nd}}(t)$ values and Neoproterozoic Hf and Nd model ages. The geochemical and isotope data suggest that ~280 Ma magmatism derived by the melting of a crustal source, induced by mantle upwelling. The ~230 Ma rock assemblage includes granitoids and volcanic rocks. The I-type calc-alkaline granitoids are enriched in K, Rb, U, and Th. The geochemical characteristics suggest that they have formed by the melting of a hornblende-bearing crustal source with the participation of fluids separated from the subducting slab. The positive $\varepsilon_{\text{Hf}}(t)$ and $\varepsilon_{\text{Nd}}(t)$ ~230 Ma rocks suggest partial melting of a depleted lower crustal material with the contribution of ancient crustal material. The ~296 Ma granitoids possess coherent/coupled Nd–Hf isotopic compositions supporting their origin from the ancient crust. Although the number of ~296 Ma samples are small, we suggest that they were probably emplaced at an active continental setting, ~280 Ma samples could have formed in a setting of local extension environment, ~230 Ma granitoids were also formed at an active continental margin. These magmatic rocks formed during the subduction of the Mongol-Okhotsk oceanic plate beneath the Central Mongolia-Erguna Block.

1. Introduction

The continental crust of the Earth is unique by the presence of

granites, compared to other planets of the solar system. Its origin and evolution have been a matter of debate among Earth scientists for a long time (Taylor and McLennan, 1995; Chen and Grapes, 2007; Pastor-Galán

* Corresponding author at: Department of Earth Science, Graduate School of Science, Tohoku University, Aoba, Sendai 980-8578, Japan.

E-mail address: ganbat.ariuntsetseg.t1@dc.tohoku.ac.jp (A. Ganbat).

et al., 2021). Granites are essential for deciphering crustal growth, tectonic evolution of the Earth and for assessing related mineral deposits (e.g., Clemens et al., 2020; Ganbat et al., 2021a). Granites and their associated volcano-plutonic suites can provide critical information about orogeny-related igneous petrogenesis and geodynamic framework (e.g., Barnes et al., 2016; Kemp et al., 2006; Pearce and Peate, 1995). The Central Asian Orogenic Belt (Fig. 1a; CAOB or Altaids) is the world largest accretionary orogenic belt sandwiched between the Siberian, Kazakhstan, Tarim, and North China continental blocks and represents the most significant juvenile crustal growth on the Earth during the Phanerozoic (e.g., Şengör et al., 1993; Kovalenko et al., 1996, 2004; Jahn, 2004; Windley et al., 2007; Xiao et al., 2010; Safonova et al., 2011,

2017; Kröner et al., 2014). Evidence for the dominantly juvenile character of the CAOB crust comes from low whole-rock initial Sr and high Nd and high Hf-in-zircon isotopic values of the CAOB igneous rocks and from the Pacific-type nature of the CAOB constituting local orogenic belts (e.g., Jahn, 2004; Safonova et al., 2011, 2017; Wilhem et al., 2012). However, the proportions of juvenile and recycled crust in the CAOB, hosting numerous volcano-plutonic complexes/suites (Fig. 1b), are still a matter of debate as many formations still lack up-to-date analytical data and many areas lack reliable tectonic models (e.g., Jahn, 2004; Kröner et al., 2014; Safonova, 2017). The solution to these problems requires reconstructing tectonic frameworks in different segments of the CAOB.

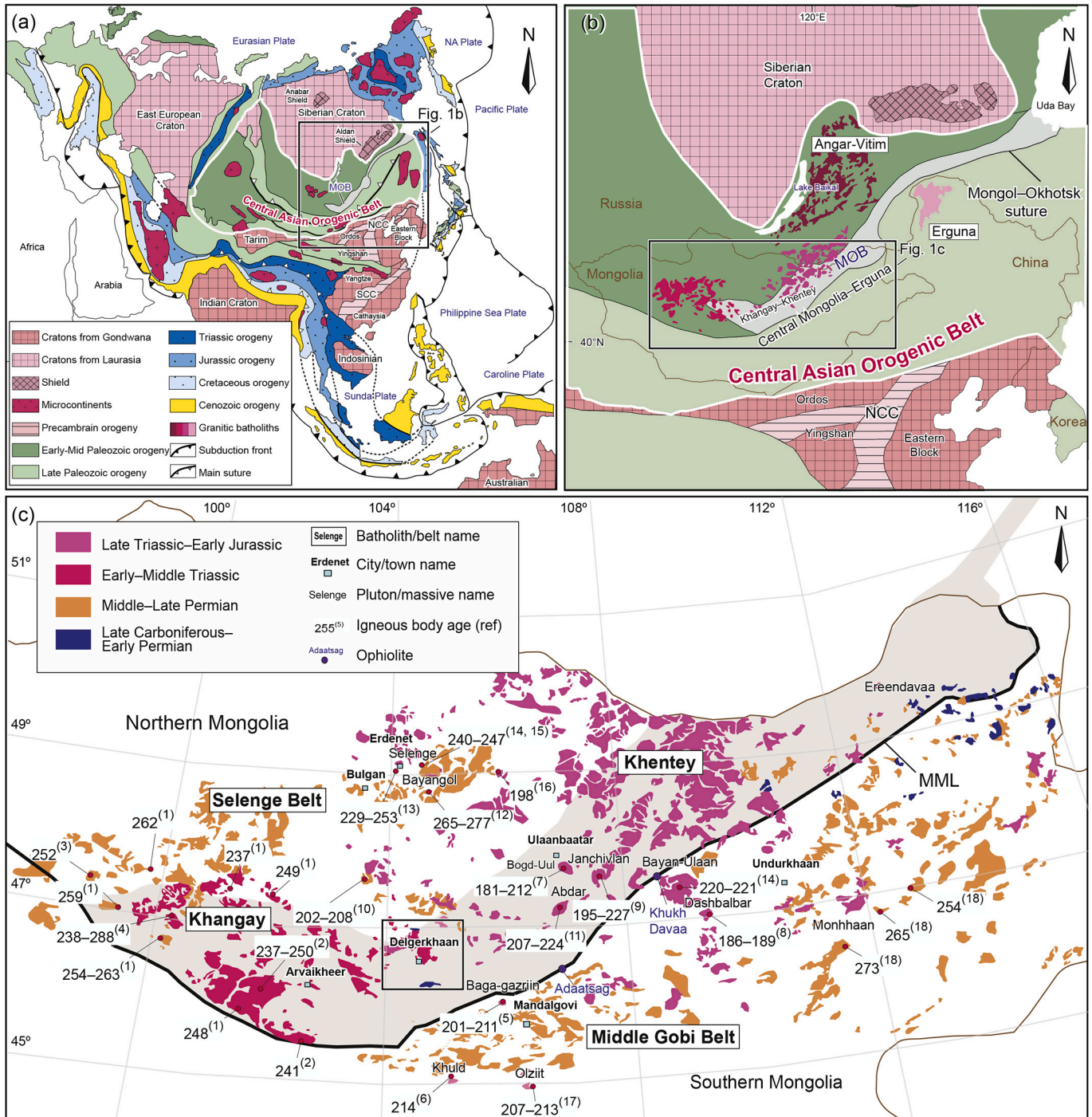


Fig. 1.

(Badarch et al., 2002; Wilhem et al., 2012). The northern domain comprises cratonic fragments, Neoproterozoic ophiolites, Precambrian and Early Paleozoic metamorphic rocks, and Early Paleozoic basins with clastic rock, island arcs, and associated volcanoclastic sediments (Badarch et al., 2002). The southern domain consists of Paleozoic island arcs, ophiolite fragments, and late Carboniferous to Permian volcanic rocks, which have been linked to the evolution of the Paleo-Asian Ocean (Kozakov et al., 2007; Lamb et al., 2001). These two domains are bounded by the Khangay-Khentei basin, part of the Mongol-Okhotsk Belt.

The Mongol-Okhotsk Belt extends over a distance of more than 3000 km from Central Mongolia to the Uda Bay in the Okhotsk Sea over the territories of Mongolia, Russia, and NE China (Fig. 1b). The Silurian to Carboniferous oceanic sedimentary sequences of the Khangay-Khentei basin (part of the Mongol-Okhotsk Belt) are overlain by Triassic terrigenous continental deposits. The Khangay-Khentei basin also includes the Adaatsag and Khuhu Davaa ophiolites with crystallization ages from 325 to 314 Ma, and associated accretionary complexes (Tomurtogoo et al., 2005; Zhu et al., 2018) marking the suture zone of the MOO (Fig. 2). The accretionary complexes include oceanic basalt (mostly OIB-type), Silurian–Devonian radiolarian pelagic chert, hemipelagic siliceous mudstone and siltstone, and trench turbidite, all elements of Ocean Plate Stratigraphy (OPS), and fore-arc greywacke sandstone (e.g., Dagva-Ochir et al., 2020; Kelty et al., 2008). The U–Pb ages of detrital zircons show that the sedimentation in the Khangay-Khentei basin began during the early Carboniferous (Kelty et al., 2008; Hara et al., 2013), and was related to coeval volcanic arc activity (Bussien et al., 2011; Ruppen et al., 2014). The general geology and the numerous intrusions of mafic to felsic igneous rocks, younging from west to east along the Mongol-Okhotsk suture (Donskaya et al., 2013), suggest that the ocean closed in a scissor-like manner during a period spanning from late Carboniferous to the Permian in central Mongolia and/or until the Triassic–early Jurassic or Cretaceous in southeastern Transbaikalia and NE China. The accurate time of its closure, however, remains uncertain (e.g., Sorokin et al., 2020). The subduction of the MOO can be responsible for the paired volcano-plutonic belts that once existed around the suture, hosting abundant granitoid intrusions: plutons with various sizes and huge batholiths. Among those are Angara-Vitim, Erguna, Khangay, and Khentei batholiths (Fig. 1b). The Angara-Vitim batholith developed on the heterogeneous basement as its granitoids yielded U–Pb ages ranging from 333 to 275 Ma (e.g., Kovach et al., 2012; Litvinovsky et al., 2011). The Erguna batholith formed in an arc and back-arc settings in the Carboniferous time (e.g., Sun et al., 2013), and continued until the early–middle Jurassic (Liu et al., 2018). The Khangay batholith is located in the western Mongol-Okhotsk Belt (Fig. 1c). It consists of several plutonic complexes formed in two phases. The first phase of granodiorite, tonalite, plagiogranite, and gabbro-diorite was followed by a second phase of biotite-tonalite, leucogranite, and alkaline granite (e.g., Yarmolyuk et al., 2016). The available U–Pb zircon, Rb–Sr isochron, and Ar/Ar ages from the Khangay batholith range from 273 to 237 Ma (Jahn, 2004; Yarmolyuk et al., 2019). The Khentei batholith is dominated by granodiorite and leucogranite with subordinate gabbro and diorite. The U–Pb zircon ages and Rb–Sr isochron ages obtained from the Khentei granitoids range from 226 to 186 Ma (Yarmolyuk et al., 2002). To the south, the Khentei batholith is bordered by abundant coeval series of bimodal volcanic rocks and alkaline Li–F granites (e.g., Yarmolyuk et al., 2002).

Of special interest is the Selenge volcano-plutonic Belt located in the northern Mongol-Okhotsk Belt (Fig. 1c) as it hosts the world-class Erdenet copper-porphyry deposit. The Selenge pluton, which is closely related to mineralization, is a composite intrusion. The oldest Selenge pluton (277–253 Ma) consists of calc-alkaline shoshonite-latitude rocks, and coeval volcanics (Munkhtsengel et al., 2007). The younger 240 Ma quartz-diorite yielded $\varepsilon_{\text{Hf}}(t)$ values from +6.9 to +14.8 and $t_{\text{Hf(DM)}}$ ages between 830 and 320 Ma. The Triassic magmatic activity formed alkaline intrusions and bimodal igneous series different from older

subduction-related magmas (Morozumi, 2003). The ore-bearing Erdenet intrusions yielded ages of 245–235 Ma and Re–Os in molybdenite yielded an age of 240 Ma (Morozumi, 2003).

The study area lays in the southern margin of the Khangay-Khentei basin, northwest of the Mongol-Okhotsk suture near the Delgerkhaan town (Fig. 2). It hosts several granitoid plutons, including undifferentiated bodies namely Batkhaan, Zambalkhudag, Delgerkhaan plutons, which are the foci of this paper. They are compositionally variable: diorite and granodiorite to subordinate monzogranite and alkaline granite (Tumurchudur et al., 2006). The Batkhaan granitoid pluton of the Permian age consists of subalkaline granite, syenogranite, quartz syenite, quartz diorite, associated with trachyrhyolite, rhyolite, and dacite. This association is overlain by the late Permian conglomerate, silicified sandstone, and siltstone strata with fauna and flora. The Delgerkhaan granitoid pluton occupies a large area and consists of calc-alkaline biotite-hornblende granite, granodiorite, monzodiorite, monzogabbro carrying mafic xenoliths (Amar-Amgalan, 2008; Tumurchudur et al., 2006). The Delgerkhaan granitoids are cut by numerous NE-trending 1–3 m wide mafic to intermediate dykes. Near the granitoid body, there are outcrops of mafic to felsic volcanic rocks. Biotite from trachyandesite yielded a K–Ar age of 223 Ma (Tumurchudur et al., 2006). According to the 1:200000 scale State Geological Map (Dagvadorj et al., 1993), the Zambalkhudag pluton consists of late Carboniferous calc-alkaline biotite-granite, granodiorite, and leucogranite. An undifferentiated smaller body, previously assumed as Cambrian granite-granodiorite, is overlain by felsic volcanogenic formations, which lithostratigraphic age is accepted as early Permian (Fig. 2; Dagvadorj et al., 1993). The igneous rocks intrude Devonian–Carboniferous dark gray sandstone, polymictic sandstone, conglomerate, gravel, and chert. In addition, there are late Triassic syenite, diorite, monzodiorite, and mafic to intermediate volcanic rocks and Cretaceous basaltic andesite—all covered by oil-bearing shale-siltstone-sandstone strata (Tumurchudur et al., 2006).

3. Analytical methods

3.1. Zircon U–Pb geochronology

Zircon crystals were separated in Tohoku University, using standard techniques including conventional rock-crushing, magnetic and heavy liquid separation, and handpicking under a binocular microscope. Then, zircon crystals were mounted in epoxy discs. Zonation of zircon interiors was documented using cathodoluminescence (CL) imaging using a Hitachi S-3400 N scanning electron microscope, equipped with a Gatan MiniCL. In-situ zircon U–Pb dating was carried out in the Okayama University of Science by using a Thermo Fisher Scientific iCAP-RQ single-collector Inductively Coupled Plasma Mass Spectrometer (ICPMS) quadrupole coupled to a Teledyne Cetac Technologies Analyte G2 ArF excimer laser ablation (LA) system equipped with a HelEx 2 volume sample chamber. The laser ablation was conducted at the laser spot size of 25 μm , the fluence of 1.8 J/cm², and the repetition rate of 5 Hz (for details see Aoki et al., 2020). NIST SRM 612 standard (Jochum et al., 2011) for instrument optimization. Reference zircon Nancy 91500 was used for age calibration (Wiedenbeck et al., 2004). ²⁰⁷Pb/²⁰⁶Pb and ²⁰⁶Pb/²³⁸U ages of Nancy 91500 zircon are 1067 \pm 4 (2 σ) and 1064 \pm 4 Ma, respectively, which are in agreement with recommended values (1065 Ma; Wiedenbeck et al., 2004). Plešovice zircons were measured as secondary standards for quality control. Measured weighted means ²⁰⁶Pb/²³⁸U age of 339 \pm 4 and ²⁰⁵Pb/²³⁵U 337 \pm 12 Ma are coincident with the reference value of Plešovice zircon (337 Ma; Sláma et al., 2008).

Zircons from samples D0815 and D0817 were analyzed for U–Pb ages at the Beijing SHRIMP Center, China, with a SHRIMP II, following the standard procedures described in (Jian et al., 2012). Prior to each analysis, the rastering of primary beams, was applied to minimize contamination by surface Pb. Reference zircon TEMORA (417 Ma; Black

et al., 2003) was used for the calibration of U concentrations and U–Pb ages, and a weighted mean value was 417 ± 3 Ma (1σ). U–Pb ages and concordia diagrams were calculated and plotted using IsoplotR software (ver. 3.75; Vermeesch, 2018); the concordia age of each sample incorporates errors on decay constants and includes evaluation of the concordance of apparent ages. The concordia ages and errors are presented at the two-sigma level.

3.2. Whole-rock geochemistry

Twenty-five samples were selected for whole-rock analysis. Concentrations of major and trace elements were measured at Activation Laboratories Ltd., Canada, using Code 4Litho LithoGeochemistry Package with fusion inductively coupled plasma optical emission spectrometry (FUS-ICPOES) and inductively coupled plasma mass spectrometry (FUS-ICPMS), respectively. Thirty-one more samples were analyzed at the Key Laboratory of Lithospheric Evolution, Institute of Geology and Geophysics, Chinese Academy of Science. Major oxides were obtained from X-ray fluorescence (XRF) with the analytical uncertainties ranging between 1 and 3%. An Inductively Coupled Plasma Mass Spectrometer (ICPMS) was used to determine rare earth elements (REE) and trace elements. The measurement error and drift were controlled by regular analysis of standard samples with a periodicity of 10%. The analyzed uncertainties of ICPMS data at the $\mu\text{g/g}$ level are better than 3–10% for the trace elements, and ~5–10% for the REE procedure at the Institute of Geology and Geophysics, Chinese Academy of Sciences. Analytical procedures are described in detail by Chu et al. (2009). Five more samples of granitoids were analyzed at the Analytical Center for Multi-Element and Isotope Studies of the Institute of Geology and Mineralogy, Novosibirsk, Russia. Major oxides were determined by the X-ray fluorescence (XRF) method using an Applied Research Laboratories ARL-9900-XP analyzer, following the standard procedure. Trace elements were analyzed by mass spectrometry with inductively coupled plasma (ICPMS) after fusion with LiBO_2 . Simultaneous determination of all elements was carried out to low, medium, and high resolution, on a Finnigan Element-II high-resolution mass spectrometer with external calibration using BHVO-1 reference samples and an internal standard. The method has been validated through the analysis of nine reference materials. Relative standard deviations for all elements were < 10% within the determined concentration ranges.

3.3. Hf-in-zircon isotopes

Zircon Hf isotope analyses were carried out using a Thermo Fisher Scientific Neptune Plus multi-collector (MC)-ICPMS in combination with a Geolas 2005 excimer ArF laser ablation system (193 nm) at the Institute of Geology and Geophysics, Chinese Academy of Science, Beijing. The analyses for zircon grains from the granites were conducted with a beam diameter of 63 μm , 6 Hz repetition rate, and an energy of 15 mJ/cm^2 . This setting yielded a signal intensity of 10 V at ^{180}Hf for the standard zircon GJ-1. The typical ablation time was 26 s, resulting in pits 20–30 μm deep. The GJ-1 zircon standard yielded an average $^{176}\text{Hf}/^{177}\text{Hf}$ ratio of 0.282000 ± 39 (2σ , $n = 10$), which was consistent with the recommended value of 0.282000 ± 5 (2σ ; Morel et al., 2008).

The initial $^{176}\text{Hf}/^{177}\text{Hf}$ ratios for the unknown samples were calculated, using the measured $^{176}\text{Lu}/^{177}\text{Hf}$ ratios, the apparent age of each zircon grain, and a ^{176}Lu decay constant of $1.867 \times 10^{-11} \text{ yr}^{-1}$ (Söderlund et al., 2004). The calculations of epsilon Hf were done using a present-day chondritic $^{176}\text{Hf}/^{177}\text{Hf}$ value of 0.282785 and $^{176}\text{Lu}/^{177}\text{Hf}$ of 0.0336 (Bouvier et al., 2008) and the present-day felsic crustal ratio of $^{176}\text{Lu}/^{177}\text{Hf} = 0.015$ (Griffin et al., 2004).

3.4. Sm–Nd isotopic analysis

Sm–Nd isotopic analyses were performed at the Institute of Precambrian Geology and Geochronology, Russian Academy of Sciences, Sankt-

Peterburg. About 100 mg of whole-rock powder was dissolved in a mixture of HF, HNO_3 , and HClO_4 . A ^{149}Sm – ^{150}Nd spike solution was added to all samples before dissolution. REEs were separated on BioRad AGW50-X8 200–400 mesh resin using conventional cation-exchange techniques. Sm and Nd were separated by extraction chromatography with a LN-Spec (100–150 mesh) resin. The total blank in the laboratory was 0.1–0.2 ng for Sm and 0.1–0.5 ng for Nd. Isotopic compositions of Sm and Nd were determined on a TRITON Thermal Ionization multi-collector mass-spectrometer (TIMS). The precision (2σ) of Sm and Nd contents and $^{147}\text{Sm}/^{144}\text{Nd}$ ratios were 0.5% and 0.005% for $^{143}\text{Nd}/^{144}\text{Nd}$ ratios. $^{143}\text{Nd}/^{144}\text{Nd}$ ratios were adjusted relative to a value of 0.512115 for the JNdi-1 standard. During the period of analysis, the weighted average of 10 JNdi-1 Nd standard runs yielded 0.512108 ± 7 (2σ) for $^{143}\text{Nd}/^{144}\text{Nd}$, normalized against $^{146}\text{Nd}/^{144}\text{Nd} = 0.7219$. The $\epsilon_{\text{Nd}}(t)$ values were calculated using the present-day values for a chondritic uniform reservoir (CHUR) $^{143}\text{Nd}/^{144}\text{Nd} = 0.512638$ and $^{147}\text{Sm}/^{144}\text{Nd} = 0.1967$ (Jacobsen and Wasserburg, 1984). Whole-rock Nd model ages $t_{\text{Hf(DM)}}$ were calculated using the model of Goldstein and Jacobsen (1988) according to which the Nd isotopic composition of the depleted mantle evolved linearly since 4.56 Ga ago and has a present-day value $\epsilon_{\text{Nd}}(0)$ of +10 ($^{143}\text{Nd}/^{144}\text{Nd} = 0.513151$ and $^{147}\text{Sm}/^{144}\text{Nd} = 0.21365$). Two-stage (crustal) Nd model ages $t_{\text{Hf(C)}}$ were calculated using a mean crustal ratio $^{147}\text{Sm}/^{144}\text{Nd}$ of 0.12.

4. Results

4.1. Petrography

The most abundant igneous rock types in the study area are granite, granodiorite, syenogranite, quartz monzonite andesite, and trachyandesite (Fig. 3). Mineral assemblages of representative samples are given in Table 1. The major constituent minerals in undifferentiated granodiorite (sample D0925) are plagioclase (~49 vol.%), quartz (~25%), K-feldspar (~25%) (Fig. 3a). The accessory minerals are magnetite, apatite, and zircon (~1%). Batkhaan inequigranular syenogranite (sample D1710) possesses hypidiomorphic texture with myrmekite intergrowths (Fig. 3b). Major minerals are anhedral quartz (~40%), euhedral to subhedral perthitic K-feldspar (phenocrysts of microcline or orthoclase in an amount of ~39%, and subhedral plagioclase (~20%). In places, the phenocrysts contain minor fractures filled by quartz and partly affected by sericitization. Zircon, apatite, opaque minerals are accessories (~1%). Batkhaan rhyolites (sample D1709) are massive and porphyritic and contain ~20% subhedral–anhedral quartz ~20% and subhedral–anhedral K-feldspar phenocrysts in a groundmass consisting of quartz, plagioclase, and K-feldspar (Fig. 3c). Delgerkhaan plutonic rocks are dominated by granite, granodiorite, and quartz monzonite. Hypidiomorphic monzogranite (sample D1742) consists of euhedral to subhedral plagioclase (~30%), subhedral K-feldspar (~30%), euhedral quartz (~20%), biotite (~13%), and hornblende (~5%), (Fig. 3d) plus accessory zircon, apatite, and titanite (~2%). Hypidiomorphic granodiorite (sample D0815) consists of plagioclase (~45%), K-feldspar (~20%), subhedral quartz (~15%), hornblende (~10%) and biotite (~8%) (Fig. 3e, f) plus accessory zircon and opaque minerals and secondary sericite and chlorite (~2%). The Zambalkhudag coarse-grained granodiorite (sample D1726) consists of subhedral plagioclase (~39%), euhedral to subhedral K-feldspar (~20%) and anhedral quartz (~20%), hornblende (~10%) and biotite (~10%) plus secondary chlorite (Fig. 3g, h). In places, plagioclase and K-feldspar form myrmekite textures. Accessory minerals are zircon and apatite (~1%). The volcanic rocks associated with the Delgerkhaan pluton are dominated by porphyry andesite and trachyandesite. Andesite (Sample D1737) contains 0.2–1 mm long subhedral phenocrysts of plagioclase (~50%) partly replaced by sericite (Fig. 3i). The groundmass (~50%) consists of K-feldspar, plagioclase laths, biotite, and secondary chlorite, and hornblende (Fig. 3i).

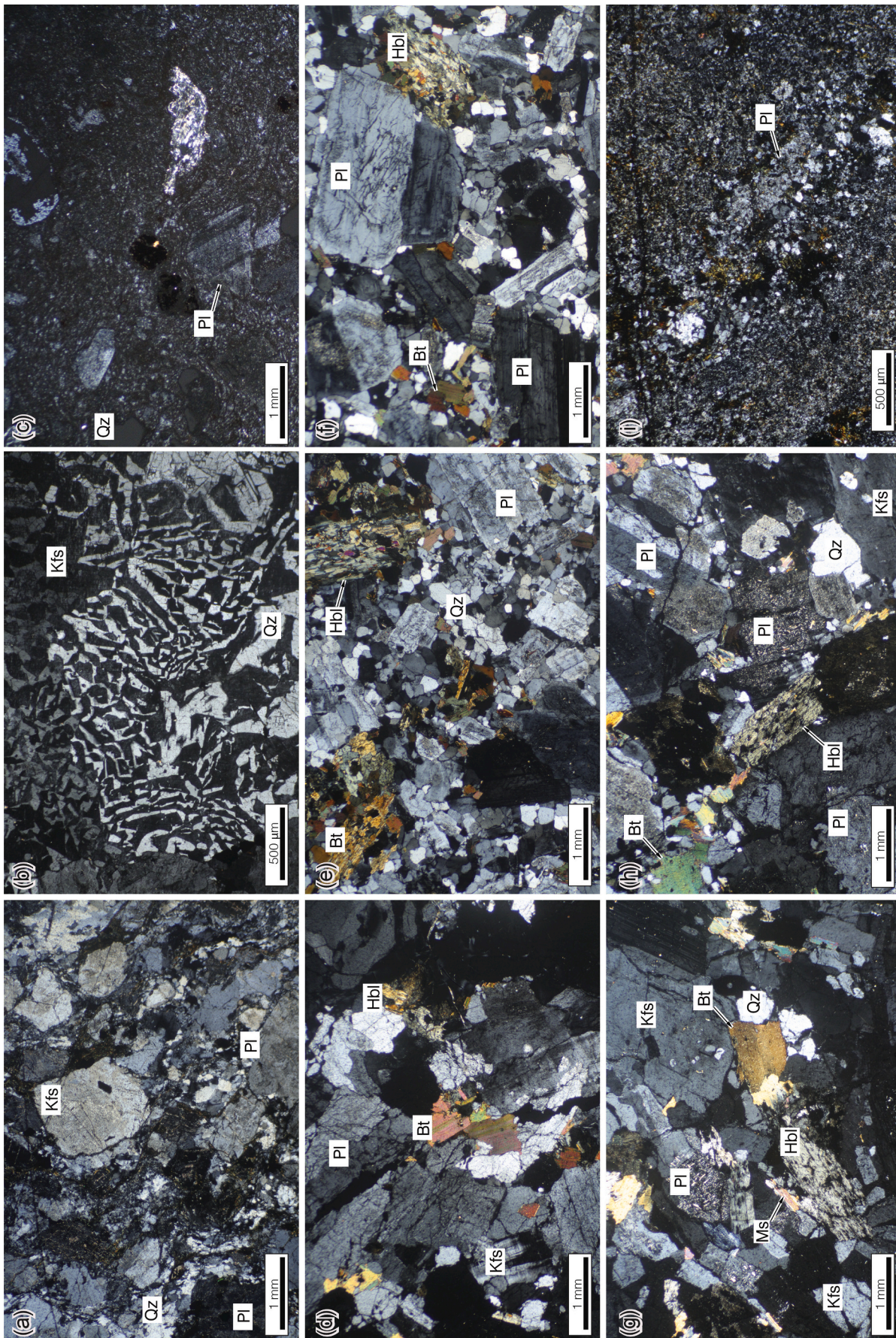


Fig. 3. Photomicrographs of cross-polarized light view showing textures and mineral assemblage of the studied samples from the Khangay-Khentei basin. (a) Granodiorite (sample D0925); (b) Syenogranite (sample D1710); (c) Rhyolite (sample D1709); (d) Monzogranite (sample D1742); (e) Granodiorite (sample D0815); (f) Granodiorite (sample D1718); (g) Monzogranite (sample D0817); (h) Granodiorite (sample D1726); (i) Andesite (sample D1745). Bt—biotite; Hbl—hornblende; Kfs—K-feldspar; Pl—plagioclase; Qz—quartz; Ms—muscovite.

Table 1
Mineral assemblage and contents of studied samples of the Khangay-Khentey basin.

No.	Sample No.	Lithology	Sampled unit	Texture	Mineral content, vol%					
					Qz	Pl	Kfs	Bt	Hbl	Accessory mineral
1	D0925	Granodiorite	Undifferentiated	Porphyritic	~25	~49	~25			~1
2	D1710-1	Monzonite	Batkhaan	Medium-grained phaneritic	~15	~59	~25			~1
3	D1710	Syenogranite	Batkhaan	Fine-grained phaneritic	~40	~20	~39			~1
4	D1707	Monzogranite	Batkhaan	Medium-grained phaneritic	~38	~30	~26	~5		~1
5	D1709	Rhyolite	Batkhaan	Porphyritic	~20		~20			~1
6	D0808	Granodiorite	Delgerkhaan	Medium-grained phaneritic	~22	~38	~25	~9	~5	~1
7	D0812	Granodiorite	Delgerkhaan	Medium-grained phaneritic	~20	~49	~20	~10		~1
8	D0815	Granodiorite	Delgerkhaan	Medium-grained phaneritic	~15	~45	~20	~8	~10	~2
9	D0817	Granodiorite	Delgerkhaan	Porphyritic	~20	~42	~20	~6	~10	~2
10	D0818	Granodiorite	Delgerkhaan	Porphyritic	~15	~50	~20	~8	~5	~2
11	D0819	Monzodiorite	Delgerkhaan	Porphyritic	~10	~48	~20	~10	~10	~2
12	D1012	Monzogranite	Delgerkhaan	Medium-grained phaneritic	~24	~30	~24	~10	~10	~2
13	D1746	Monzogranite	Delgerkhaan	Medium-grained phaneritic	~25	~40	~20	~14		~1
14	D1742	Monzogranite	Delgerkhaan	Medium-grained phaneritic	~20	~30	~30	~13	~5	~2
15	D1718	Monzogranite	Delgerkhaan	Medium-grained phaneritic	~25	~30	~29	~5	~10	~1
16	D1726	Granodiorite	Zambalkhudag	Medium-grained phaneritic	~20	~39	~20	~10	~10	~1
17	D1737	Andesite	Triassic volcanic	Massive		~50				~1

4.2. U–Pb geochronology

The separated zircon grains are stubby to elongated and euhedral to subhedral. Their sizes range from 50 to 300 μm and the aspect ratio varies from 1.5 to 3. The grains are transparent, mostly colorless or yellowish to brownish. In CL images most grains exhibit fine to coarse banded oscillatory zoning (Fig. 4), although there are also zircons with patchy or sectorial zoning. Sample D0925 was collected from an undifferentiated granitoid body. It yielded one zircon grain with an age of 498 Ma, while the rest zircons are 296 ± 3 Ma (Fig. 5). Samples D1710 and D1709 were collected from the Batkhaan suite and carry zircons with U–Pb concordia ages of 274 ± 3 to 282 ± 2 Ma. Samples D1742, D0815, D0817, D1718, and D1726 were taken from the Delgerkhaan and Zambalkhudag plutons, and their zircon concordia ages are bracketed between 220 ± 2 Ma and 240 ± 3 Ma. Table 2 presents zircon features of each sample and their yielded ages. Zircon dating results are shown in Supplementary Table 2. Our new U–Pb age results allow us to highlight three groups of magmatism in the Delgerkhaan area from the early Permian until the late Triassic at ~ 296 , ~ 280 , and ~ 230 Ma.

4.3. Whole-rock geochemistry

4.3.1. ~ 296 Ma granitoids

The major and trace element geochemical data of the studied samples are given in Supplementary Table 3. The undifferentiated granitoids of the study area are characterized by medium SiO_2 (65.7–66.7 wt%), Al_2O_3 (15.0–16.7 wt%), and low TiO_2 (0.39–0.61 wt%). The contents of MgO and FeO^{T} range from 0.61 to 1.29 and from 2.58 to 3.94 wt%, respectively, resulting in Fe numbers of 0.75 to 0.83 [$\text{Fe}\# = \text{FeO}^{\text{T}} / (\text{FeO}^{\text{T}} + \text{MgO})$] and Mg numbers of 44 to 56 [$\text{Mg}\# = \text{molar } 100 \times \text{Mg} / (\text{Mg} + \text{Fe})$]. The total alkalis ($\text{Na}_2\text{O} + \text{K}_2\text{O}$) are high (7.9–8.3 wt%), in the TAS diagram they plot in the field of quartz monzonite (Fig. 6a). The rocks are ferroan to magnesian (Fig. 6c) and high-K calc-alkaline (Fig. 6d). They belong to I-type granites, and the ratio of A/CNK [molar $\text{Al}_2\text{O}_3 / (\text{CaO} + \text{K}_2\text{O} + \text{Na}_2\text{O})$] ranges from 0.94 to 1.04 indicating their metaluminous to the weakly peraluminous character (Fig. 7c). The rocks exhibit high concentrations of Sr and low concentrations of Y and Yb. In addition, they have low Cr, and Ni. The degree of LREE and HREE differentiation is moderate to high with $(\text{La}/\text{Yb})_{\text{CN}} = 11\text{--}32$ (Fig. 8a). The REE patterns show weak negative to zero Eu anomalies. The primitive mantle-normalized multi-element patterns show enrichment in incompatible elements and positive Nb, Ta anomalies relative to Th and La (Fig. 8b).

4.3.2. ~ 280 Ma volcanoplutonic rocks

The ~ 280 Ma pluton consist of granites and monzonites (Fig. 6a). The SiO_2 content of the Batkhaan granitoids span between 72.9 and 77.2 wt%, and total alkalis are 7.46–9.77 wt%. The rocks have low Al_2O_3 (11.3–14.9 wt%), Mg# (14–39), and CaO (0.08–0.78 wt%), but high Fe# (0.86–0.96 wt%), i.e., they represent ferroan rocks and normal to high-K calc-alkaline (Fig. 6c, d). Compared to the granites, the monzonites have lower SiO_2 (59.5–61.4 wt%) and total alkalis (6.86–7.72 wt%), but higher Al_2O_3 (16.6–19.7 wt%) and Mg# (26–36) and CaO (3.4–5.9 wt%). The volcanic rocks are dominantly rhyolite except for one sample of dacite (Fig. 6b). They belong to A-type granites (Fig. 7a, b) and their A/CNK values range from 0.95 to 1.13, indicating peralkaline, metaluminous, and peraluminous transition character (Fig. 7c). They have high $\text{SiO}_2 = 67.9\text{--}77.6$ wt%, and total alkalis = 6.5–8.8 wt%, but low Al_2O_3 (11.2–13.6 wt%), Mg# (10–39), and CaO (0.05–1.75 wt%). All ~ 280 Ma rocks, both plutonic and volcanic, have slightly LREE enriched [$(\text{La}/\text{Yb})_{\text{CN}} = 2.8\text{--}6.6$, except D1721 = 23.5] with clear Eu troughs (Fig. 8c). They are enriched in Nb, Zr, Y, and U, but depleted in Sr (17–263 $\mu\text{g}/\text{g}$ in granites and 245–456 $\mu\text{g}/\text{g}$ in monzonites). The primitive mantle normalized spidergrams of the ~ 280 Ma rocks show deep troughs at Ba, Sr, P, Eu, and Ti and shallower troughs at Nb, Ta (Fig. 8d).

4.3.3. ~ 230 Ma volcanoplutonic rocks

Previous researchers considered the Delgerkhaan and Zambalkhudag plutons as different bodies (Tumurchudur et al., 2006). In this paper, we characterize them together since they possess similar geochemical features. These ~ 230 Ma rocks of the Delgerkhaan and Zambalkhudag plutons span wide ranges of SiO_2 (61.4–75 wt%) and total alkalis ($\text{Na}_2\text{O} + \text{K}_2\text{O} = 6.3\text{--}9.4$ wt%), a restricted range of Al_2O_3 (12.9–16.60 wt%). Most of the samples are characterized by high TiO_2 (0.03–0.82 wt%), moderate FeO^{T} (1.0–5.3 wt%), and high Mg# (44–73) except for three samples with lower Mg# (2.85–24). In the TAS diagram, the granitoids fall in the fields of granodiorite, quartz monzonite, and granite (Fig. 6a). As Fe# ranges from 0.53 to 0.99, the granitoids belong to the magnesian type and high-K calc-alkaline series granites (Fig. 6c, d). The samples plot on the I-type granite field (Fig. 7a, b) and in the A/CNK versus A/NK diagram, the samples plot in the metaluminous and I-type fields (Fig. 7c, d). The chondrite normalized REE patterns show less fractionated HREE, and weak to zero negative or positive Eu anomalies (Fig. 8e). The spidergrams show enrichment in LILEs and depletion in HFSEs. They display lower contents of Nb, Zr, Y, and U, but higher Sr and Pb (Fig. 8f). The samples are characterized by high Sr, and low Y, and Yb. The volcanic rocks associated with the Delgerkhaan pluton have $\text{SiO}_2 = 58.5\text{--}68.1$, $\text{MgO} = 0.50\text{--}7.4$, $\text{Al}_2\text{O}_3 = 13.6\text{--}16.2$, $\text{TiO}_2 = 0.6\text{--}1$ wt%,



Fig. 4. Cathodoluminescence (CL) images of representative zircon crystals from the studied samples from the Khangay-Khentyey basin. White circles show individual analysis spots, corresponding U–Pb ages and yellow circles show an individual spot of Lu–Hf isotope and their $\epsilon_{\text{Hf}}(t)$ values. (For interpretation of the references to color in this figure legend, the reader is referred to the web version of this article.)

$\text{FeO}^{\text{T}} = 4.16\text{--}7.4$, $(\text{Na}_2\text{O} + \text{K}_2\text{O}) = 5.18\text{--}8.6$ wt%. The values of Mg# and Fe# are bracketed between 22 and 79, 0.5 and 0.93, respectively. The volcanic rocks are andesite, trachyandesite, trachydacite, and dacite (Fig. 6b). According to A/CNK (0.77–1.07), they represent metaluminous to peraluminous varieties (Fig. 7c). The chondrite normalized REE patterns (Fig. 7a) show enrichment in LREEs $[(\text{La}/\text{Yb})_{\text{CN}} = 2.88\text{--}34.6]$, and weak negative to positive Eu anomalies. The multi-element patterns show negative Nb, Ta, and Ti anomalies (Fig. 8f) and significant enrichment in LILE (K, Rb, Ba, Sr) (Fig. 8f).

4.4. Zircon Hf isotopes

Seven analyses from ~ 296 Ma intrusion sample gave initial $^{176}\text{Hf}/^{177}\text{Hf}$ ratios ($t = 296$ Ma) varying from 0.282488 to 0.282654, among which one analysis on an inherited zircon grain with an age of ~ 498 Ma yielded initial $^{176}\text{Hf}/^{177}\text{Hf}$ ratios ($t = 498$ Ma) of 0.282488 (Supplementary Table 4). Their $\epsilon_{\text{Hf}}(t)$ values and two-stage model $t_{\text{Hf}(C)}$ ages range from -2.3 to $+2.6$ and from 1168 to 1527 Ma, respectively. The initial $^{176}\text{Hf}/^{177}\text{Hf}$ ratios for 15 spots of the ~ 280 Ma volcanoplutonic rocks (samples D1710 and D1709) vary from 0.282664 to 0.282918, respectively. The corresponding $\epsilon_{\text{Hf}}(t)$ values and two-stage model ages $t_{\text{Hf}(C)}$ vary from $+2.1$ to $+11.2$ and 581 to 1159 Ma, respectively. Twenty-one analyses of three samples from the ~ 230 Ma volcanoplutonic rocks (samples D1718, D1726, and D1742) yielded initial $^{176}\text{Hf}/^{177}\text{Hf}$ ratios from 0.282684 to 0.282830, which are translated into $\epsilon_{\text{Hf}}(t)$ values from $+1.9$ to $+7.1$ and $t_{\text{Hf}(C)}$ between 810 and 1139 Ma, respectively.

4.5. Sm–Nd isotopic analysis

The Sm–Nd isotopic analysis was carried out for 5 selected samples. One sample from each granitic massif, and one from the ~ 280 Ma rhyolite. The $\epsilon_{\text{Nd}}(t)$ values are calculated using the zircon U–Pb concordant ages of each sample. The sample from ~ 296 Ma granitoid has $\epsilon_{\text{Nd}}(t) = -1.7$ and corresponds to $t_{\text{Nd}(\text{DM})} = 1076$ Ma (Supplementary Table 4). The ~ 280 Ma volcanic and plutonic rocks have higher $\epsilon_{\text{Nd}}(t)$ values varying from $+2.7$ to $+4.1$. They have $t_{\text{Nd}(\text{DM})}$ model ages of 762–993 Ma. The remained samples exhibit $\epsilon_{\text{Nd}}(t)$ values ranging from -0.7 to $+1.7$ corresponding to $t_{\text{Nd}(\text{DM})}$ model ages of 697–1509 Ma.

5. Discussion

5.1. Emplacement ages of the Late Paleozoic–Early Mesozoic felsic-intermediate magmatism

Our U–Pb age results allow us to recognize three groups of magmatism in the Delgerkhaan area from the late Permian until the late Triassic: at ~ 296 , ~ 280 , and ~ 230 Ma. The ~ 296 Ma intrusion was previously considered as late Cambrian (Dagvadorj et al., 1993), but our new data show that it has early Permian age. Moreover, the granitoids contain late Cambrian (Furongian) inherited zircon (498 Ma), implying that melt incorporated zircons that crystallized in the past. The ~ 280 Ma magmatism formed the Batkhaan granites, monzonites, and associated rhyolites of 282 ± 3 and 274 ± 2 Ma, respectively (Fig. 5). These ages are consistent with the lower precision age of 282 ± 16 Ma previously reported (Amar-Amgalan, 2008). The area of the ~ 230 Ma plutons includes the Delgerkhaan pluton emplaced at 230–240 Ma. The Zambalkhudag pluton, previously thought to be late Carboniferous, since it intrudes Devonian sandstones (Tumurchudur et al., 2006 and reference therein), actually formed at 220 ± 2 Ma. We suggest that the Zambalkhudag pluton is almost coeval and related to the Delgerkhaan pluton as they possess similar geochemical and isotope characteristics and show similar ages of crystallization (Table 2; Figs. 5, 8). The ~ 230 Ma magmatism also generated the associated ~ 223 Ma (K–Ar) intermediate volcanics (Dagvadorj et al., 1993).

5.2. Petrogenesis and sources

5.2.1. ~ 296 Ma granitoids

The ~ 296 Ma granitoids are metaluminous to peraluminous and have an I-type trend in the Th versus Rb diagram (Figs. 6, 7c). Two samples have elevated Rb, K, U, and Th concentrations and low MgO, Cr, and Ni contents implying crustal compositional affinities. In addition, the values of Nb/Ta (9.4–11) and Zr/Hf (38–39) differ from those of the primitive mantle (Nb/Ta = 17.8; Zr/Hf = 45; Green, 1995), and closer to the crustal values (Nb/Ta = 11; Zr/Hf = 33; Rudnick and Gao, 2003),

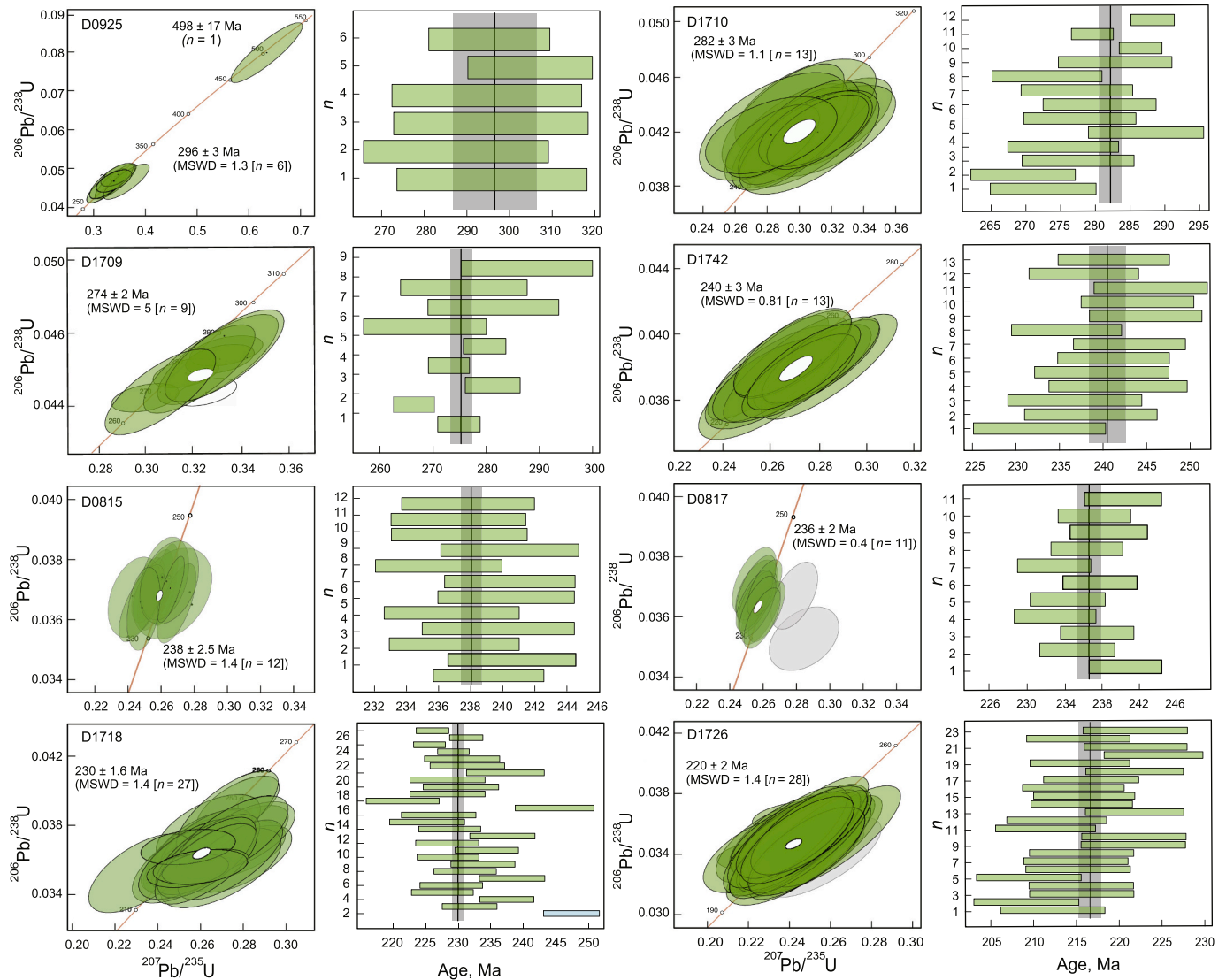


Fig. 5. Concordia diagrams of zircons for samples from the Khangay-Khenty basin, showing U–Pb isotope ratios. Light grayish ellipses indicate discordant data excluded from the calculation. Sample D0925 is classified as ~296 Ma, samples D1710 and D1709 are classified as ~280 Ma and samples D1742, D0815, D0817, D1718 are classified as ~230 Ma.

thereby supporting a crustal source for their parental magma. Their chondrite-normalized REE patterns are enriched in the LREEs, depleted in the HREEs, and show no Eu and Sr anomalies (Fig. 8a) precluding fractionation of plagioclase. The primitive-mantle normalized multi-element patterns show pronounced negative anomalies at Nb, and Ti (Fig. 8b), which are typical of supra-subduction igneous rocks. Nevertheless, one sample has low K_2O , U, Th, and their Nb/Ta (16) and Zr/Hf (45) ratios are closer to those of the primitive mantle. Although the number of samples is not enough to discuss their petrogenesis in detail, we suggest that the ~296 Ma granitoids derived from two types of source: felsic (recycled) and mafic (mixed or juvenile). The two samples of ~296 Ma granitoids have mostly negative values of $\varepsilon_{\text{Nd}}(t)$ (–1.7) and $\varepsilon_{\text{Hf}}(t)$ (–3.5 to +2.3), and Neoproterozoic to Mesoproterozoic model ages implying the presence of an older crust material in their source (Fig. 9a, b). The coupled and enriched Nd–Hf isotope compositions support that these samples are related to the partial melting of crustal rocks (Hoffmann et al., 2011).

5.2.2. ~280 Ma volcanic and plutonic rocks

We consider that all coeval ~280 Ma granitoids and rhyolites are tectonically related due to their similar ages and geochemical features

(Figs. 6, 7; Supplementary Table 3). The ~280 Ma rock association is characterized by high total alkalis, Fe#, Ga/Al, HFSEs (Zr, Nb, and Y) and REEs low CaO, Ba, and Sr, and clear negative Eu anomaly (Fig. 8c, d). These features suggest that they have characteristics similar to A-type granites (Fig. 7a, b). The origin, evolution, and tectonic settings of formation/emplacement of A-type granites remain debatable, though (e.g., Bonin, 2007). They can be produced by: (1) fractionation of mantle-derived magmas with or without interaction with crustal rocks (Turner et al., 1992); (2) low degrees of partial melting of lower crustal or underplated basaltic magma (Jones et al., 2018); (3) hybrid magma from the mantle and crustal derived melts and metasomatism of granitic magmas (Taylor and McLennan, 1995).

The ~280 Ma rocks show no coeval mafic igneous rocks, as should be expected for extensive fractional crystallization. Restricted variations of zircon $\varepsilon_{\text{Hf}}(t)$ values exclude the mixing of mantle-derived and crust-derived melts as that would have generate melts with scattered isotopic signatures (e.g., Kemp et al., 2007). The low Nb, and Ti and high Th, U, and Pb contents, high trace element ratios of Th/Ce (0.18–0.31) and Th/La (0.4–0.86) ratios suggesting a significant contribution of the continental crust during their generation. The monzonites of ~280 Ma rocks show different geochemical characteristics, such as the lack of Eu

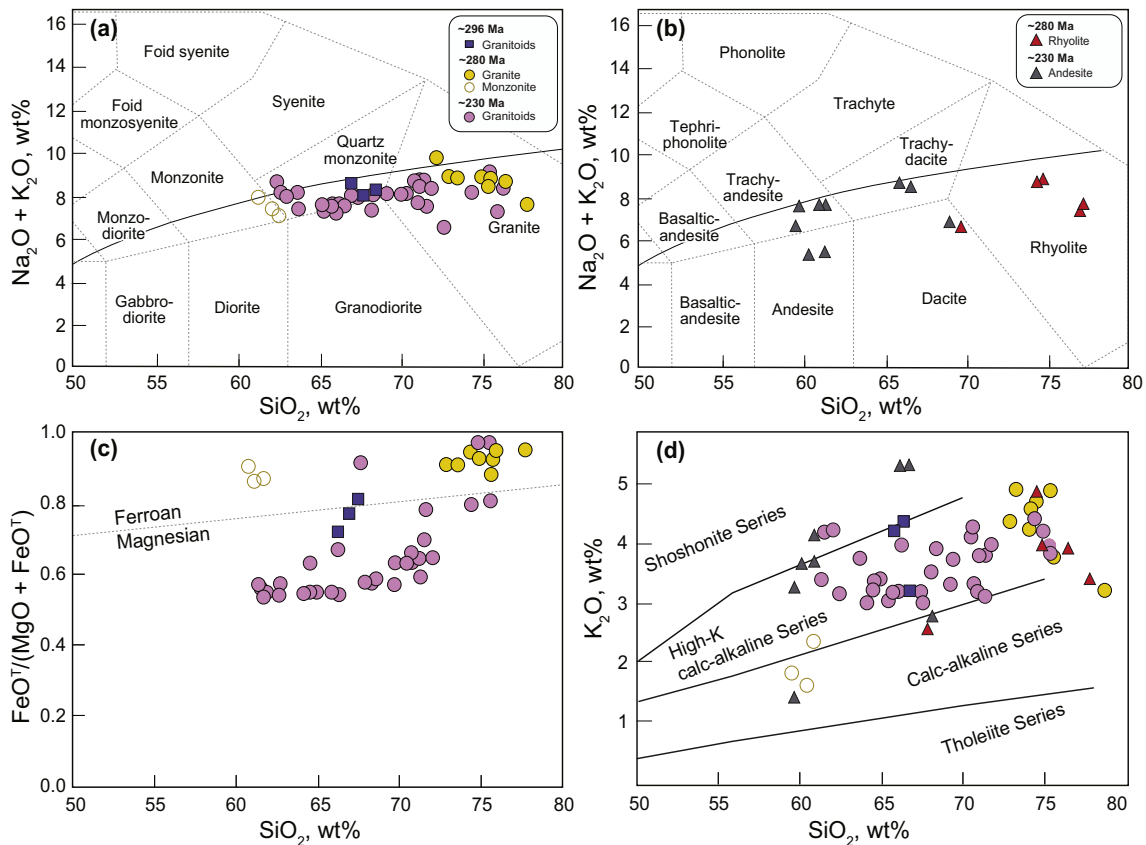


Fig. 6. Major element discrimination diagrams showing the compositions and characteristics of the studied samples from Khangay-Khentei basin, Central Mongolia. (a) SiO_2 versus $(\text{Na}_2\text{O} + \text{K}_2\text{O})$ total alkali-silica (TAS) diagram for plutonic rocks (after Irvine and Baragar, 1971), (b) SiO_2 versus $(\text{Na}_2\text{O} + \text{K}_2\text{O})$ total alkali-silica (TAS) diagram for volcanic rocks (after Le Bas et al., 1986), (c) $\text{FeO}^T/(\text{MgO} + \text{FeO}^T)$ wt% versus SiO_2 wt% plot (after Frost et al., 2001), (d) K_2O wt% versus SiO_2 wt% plot (Peccerillo and Taylor, 1976).

anomaly, the low contents of K_2O , Th and Rb, and Th/Ce (0.11–0.14) and (Th/La) (0.24–0.29) ratios lower than those in granites and rhyolites and closer to those of basaltic rocks (Rudnick and Gao, 2003). We suggest that the ~280 Ma monzonites were formed through the partial melting of a mafic source.

Experimental data indicate that metaluminous and peraluminous A-type magmas like ~280 Ma granites and rhyolite samples can be produced by the melting of calc-alkaline tonalite and granodiorite at shallow depths (4 kbar) and high temperatures (950 °C) (Patiño Douce, 1997). In fact, the low $(\text{La}/\text{Yb})_{\text{CN}}$ ratios as well as the pronounced negative anomalies of Ba, Eu, and Sr (Fig. 8c, d) of ~280 Ma rhyolites and granites with metaluminous to peraluminous compositions indicate that they formed at shallow crustal depths (Bonin, 2007). ~280 Ma rocks exhibit the positive value of $\varepsilon_{\text{Hf}}(t)$ (+2.1 to +9.7) and $\varepsilon_{\text{Nd}}(t)$ (+2.7 to +4.1) (Fig. 8b) and corresponding two-stage model ages suggesting that these rocks were generated from a Neoproterozoic juvenile source. The high temperatures of melting required to produce A-type rocks were probably provided by the underplating of juvenile mafic magmas, which fed the melting of the monzonites in the lower crust and granites and rhyolites at a shallow crustal depth.

5.2.3. ~230 Ma volcanoplutonic rocks

The ~230 Ma volcanic and plutonic rocks are calc-alkaline and have high-K, Rb, U, and Th (Figs. 6d; 8e, f). However, compared to ~296 Ma granitoids, the ~230 Ma samples have higher Mg, Cr, and Ni, suggesting a deeper and/or more mafic source of melting. The absence of contemporaneous mafic microgranular enclaves excludes extremal fractional crystallization of mantle-derived magma. Their high Sr/Y ratio and fractionated REE pattern suggest the presence of minerals with high partition coefficients for HREE, i.e., garnet or hornblende, in the

residue. The melts that equilibrate with residual garnet would have steep HREE distribution patterns and a high ratio of Yb/Lu (>10; Moyen, 2009). However, the ~230 Ma rocks show moderately steep REE distribution patterns (Fig. 8e, f) and relatively low Yb/Lu (5–7) ratios excluding the presence of garnet in the residue. The REE patterns of the ~230 Ma volcanic and plutonic rocks are moderately concave-upward between the MREEs and HREEs (Fig. 8e), which is typical for hornblende-bearing sources as hornblende preferentially incorporates MREEs over HREEs (Macpherson et al., 2006). The low Nb/Ta and SiO_2 (Fig. 10a) can also be explained by the fractionation of hornblende as such decreases Nb/Ta ratios in evolved melts (Tiepolo and Vannucci, 2014). More evidence for the fractionation of hornblende comes from the Dy versus Er diagram (Fig. 10b) showing a positive correlation between these two elements, which implies fractionation of hornblende during magmatic evolution because Er and Dy have similar values of partition coefficient in felsic magmas (Tiepolo et al., 2007).

The values of Fe# in the ~230 Ma rocks are relatively low (average = 0.68) compared to other groups of samples (Fig. 6c; Frost et al., 2001). Such low Fe# granitoids are common in the Cordilleran batholiths (<0.6) and even in the Caledonian post-orogenic granites (~0.5). As Fe# is strongly affected by differentiation during magma ascent (Frost et al., 2001), and early crystallization of Fe-bearing mineral phases would inhibit iron enrichments during differentiation. In case of ~230 Ma granitoids, we suggest that fractional crystallization of hornblende provided the formation of peraluminous I-type granitoids with lower Fe# (Chappell et al., 2012).

Diagrams La/Yb versus La and Zr/Nb versus Zr can be used to evaluate the effect and degree of fractional crystallization and partial melting on compositional variations in magmas. The samples are forming trend parallel to the array of partial melting (Fig. 11a, b)

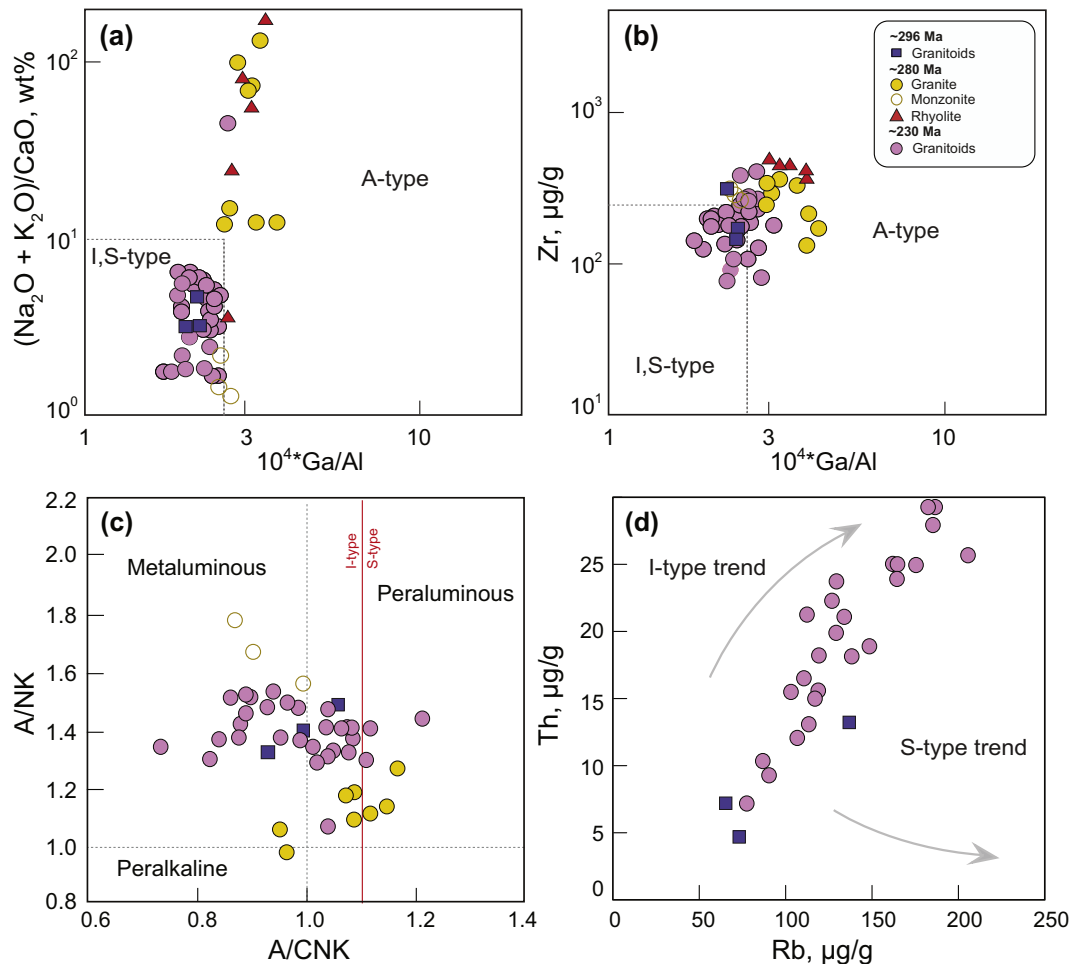


Fig. 7. (a) $(\text{Na}_2\text{O} + \text{K}_2\text{O})/\text{CaO}$ versus $10^4 \times \text{Ga}/\text{Al}$ and (b) Zr versus $10^4 \times \text{Ga}/\text{Al}$ plots (after Whalen et al., 1987) discriminating A-type granites from I, S type granites; (c) A/NK [molar $\text{Al}_2\text{O}_3/(\text{CaO} \times \text{Na}_2\text{O} \times \text{K}_2\text{O})$] versus A/NK [molar $\text{Al}_2\text{O}_3/(\text{Na}_2\text{O} \times \text{K}_2\text{O})$] diagram, the boundary line is from Maniar and Piccoli (1989); (d) Rb versus Th diagrams for the studied samples from the Khangay-Khenty basin.

suggesting that partial melting played a greater role than fractional crystallization. The Nb/Zr versus Th/Zr (Fig. 11c) and Nb/Y versus Rb/Y (Fig. 11d) systematics also confirm the participation of subducted slab-derived fluids during the magma generation.

The combination of these features with the enrichment of ~ 230 Ma rocks in LREEs and LILEs and depletions in HREEs and HFSEs (Fig. 8e, f) suggests that these rocks resulted from the partial melting of lower crustal source with hornblende in residue and participation of subduction-related fluids. As the ~ 230 Ma samples are characterized by positive $\varepsilon_{\text{Hf}}(t)$ and positive to negative $\varepsilon_{\text{Nd}}(t)$ (Fig. 9a, b), and Neoproterozoic two-stage model ages, we conclude that their primary magma originated by the partial melting of Neoproterozoic depleted lower crust (Fig. 12a, b).

5.3. Tectonic model

The geochemical and isotope compositions of the three groups of igneous rocks of the Khangay-Khenty basin in the Central Mongolia suggest different tectonic settings of their emplacement. Although we have data from three ~ 296 Ma samples only, they are plotted in the fields of volcanic arc and active continental margin in the Nb versus Y (Fig. 13a) and Th/Yb versus Ta/Yb (Fig. 13b) diagrams, respectively. As they have non-radiogenic Hf - Nd composition (Fig. 9), we suggest that they were emplaced in an active continental margin setting.

On the tectonic discrimination Nb versus Y and Rb versus $\text{Y} + \text{Nb}$ diagrams, most samples of ~ 280 Ma volcanoplutonic rocks plot in the

field of post-collisional granites (Fig. 13a). However, the post-collisional setting is an unlikely hypothesis since, so far, no evidence of collision has been found in the adjacent areas, e.g., significant crustal thickening, abundant S-type granites, etc. Moreover, the amount of outcropped A-type granites and rhyolites in the study area is relatively small, although post-collisional settings are characterized by compositionally variable, and a huge volume of granitoids. The ~ 280 Ma rocks show high Ce/Nb , Y/Nb , and Ga/Nb ratios and therefore represent A_2 -type granitoids (Fig. 14a, b). Felsic igneous rocks formed at convergent margin settings may also exhibit A-type signatures. For example, the A-type granites of the Lachlan Belt in eastern Australia were emplaced in a back-arc extensional setting in response to the slab roll-back of pre-existing subduction (e.g., Collins et al., 2020). Although the petrogenesis of ~ 280 Ma samples (A_2 -type) may support such a scenario, we think that the magmatism found is not sufficiently important. Usually, such a back-arc extension setting is predated by a vast subduction-related granitoid batholiths emplacement, like those of the Eastern Sikhote-Alin or the Andes (Dahlquist et al., 2010; Grebennikov et al., 2016). The outcrop of the ~ 296 Ma granitoids are small and pre-early Permian granitic bodies are scarce in Central Mongolia as well (Fig. 1c). Therefore, we assume that the ~ 280 Ma rocks emplaced in a setting of local extension possibly linked with magma underplating and/or asthenosphere upwelling.

The ~ 230 Ma high-K calc-alkaline I-type granitoids with low $\text{Fe}\#$ could be emplaced in two tectonic settings: (1) Andean-type active continental margin, (2) post-collisional (Frost et al., 2001). The ~ 230 Ma granites are compositionally close to andesite and trachyandesite

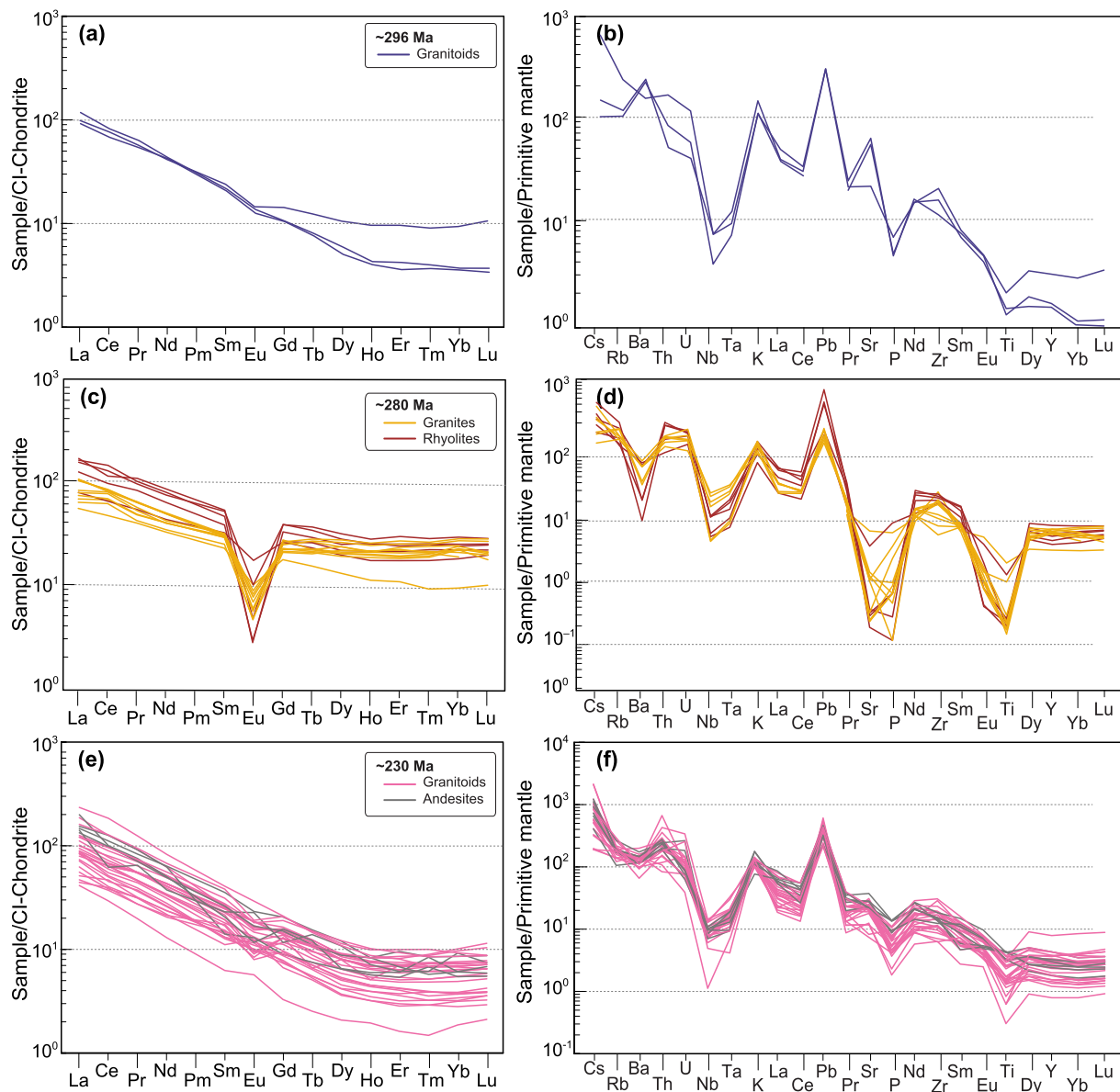


Fig. 8. CI-chondrite-normalized REE patterns and primitive-mantle-normalized trace element spidergrams for the studied samples from the Khangay-Khentei basin. Both chondrite and primitive-mantle normalized values are from Sun and McDonough (1989).

(Fig. 2), and enriched in LREEs and LILEs, but depleted in HFSEs (e.g., Nb and Ti) (Figs. 7, 8). In the Nb versus Y (Fig. 13a) and Th/Yb versus Ta/Yb (Fig. 13b) diagrams, they plot in the volcanic arc granite field and active continental margin field, respectively. These characteristics suggest their emplacement in a subduction-related tectonic setting, although post-collisional granites also show arc-like trace element signatures due to the contribution of subduction-related materials from previous tectonic events. However, recent studies have shown that the Mongol-Okhotsk Ocean remained open until the Middle Triassic. The evidences for this comes from: (1) Middle Triassic subduction-related magmatism manifested on its both sides, northern (e.g., Donskaya et al., 2013) and southern (e.g., Liu et al., 2018; Zhu et al., 2016); (2) zircon ages from metasediments (turbiditic and greywacke sandstones) in the eastern part of the Mongol-Okhotsk Belt, which peak at ~173 Ma, indicating that sedimentation of the Mongol-Okhotsk oceanic basin continued until the middle Jurassic (e.g., Sorokin et al., 2020); (3) paleomagnetic data from the volcanic rocks of NE Mongolia reveal that the Central Mongolia Block was separated from the Siberian Craton by the MOO with a ~30° latitudinal difference in the early Permian and

welded in the middle Jurassic (e.g., Yi and Meert, 2020); (4) coexistence of Boreal-type realm (northern cold affinity) and Tethyan-type realm (southern warm affinity) Anisian (Middle Triassic) ammonoid fauna in the Khentei province suggests that a wide ocean still existed during the Middle Triassic (Ehiro et al., 2006). The study area lies about 150 km to the west from Adaatsag ophiolite—a suture of the Mongol-Okhotsk Ocean. Besides, the study area is adjacent to the Central Mongolia-Erguna Block from the south (e.g., Wilhem et al., 2012). Therefore, present-day data do not support a post-collisional origin for ~230 Ma rocks. Consequently, we think that an Andean-type active continental margin explains better the characteristics of ~230 Ma volcanoplutonic rocks.

5.4. Geodynamic implications

The three groups of magmatic felsic rocks that crop out in the Khangay-Khentei basin of Central Mongolia formed during the Late Paleozoic to the Early Mesozoic in different tectonic settings. The late Carboniferous and early Permian tectono-magmatic activity in the

Table 2
Summary of zircon characteristics of dated samples and corresponding ages.

No	Sample No.	Rock type	Technique	Geological age	Grain shape	Grain size, μm	Grain color	CL feature	Th/U ratio	Concordia age, Ma	<i>n</i>	MSWD
1	D0925	Granodiorite	LA-ICPMS	Late Cambrian	stubby	up to 200	light brown, yellow	patchy zoning	0.39–1.1	296 ± 3	6	1.3
2	D1710	Syenogranite	LA-ICPMS	Late Permian–Early Triassic	mostly stubby	~150	mostly yellow	faint oscillatory	0.68–1.1	282 ± 3	13	1.1
3	D1709	Rhyolite	LA-ICPMS	Late Permian–Early Triassic	mostly stubby	~150	mostly yellow	faint oscillatory	0.84–1.3	274 ± 2	9	5
4	D1742	Monzogranite	LA-ICPMS	Late Permian–Early Triassic	mostly elongated	up to 300	mostly clear	wide oscillatory, sector	0.4–0.9	240 ± 3	13	0.81
5	D0815	Granodiorite	SHRIMP	Late Permian–Early Triassic	stubby to elongate	up to 300	clear, light brown	wide oscillatory	0.31–0.8	238 ± 2.5	12	1.4
6	D0817	Granodiorite	SHRIMP	Late Permian–Early Triassic	mostly stubby	up to 200	clear, light brown	wide oscillatory	0.53–0.8	236 ± 2	11	0.4
7	D1718	Monzogranite	LA-ICPMS	Late Permian–Early Triassic	mostly elongated	up to 300	clear, light brown	Oscillatory, patchy	0.44–1.07	230 ± 1.6	27	1.4
8	D1726	Granodiorite	LA-ICPMS	Late Carboniferous	mostly elongated	100–300	mostly clear	Oscillatory	0.4–1.2	220 ± 1	28	1.4

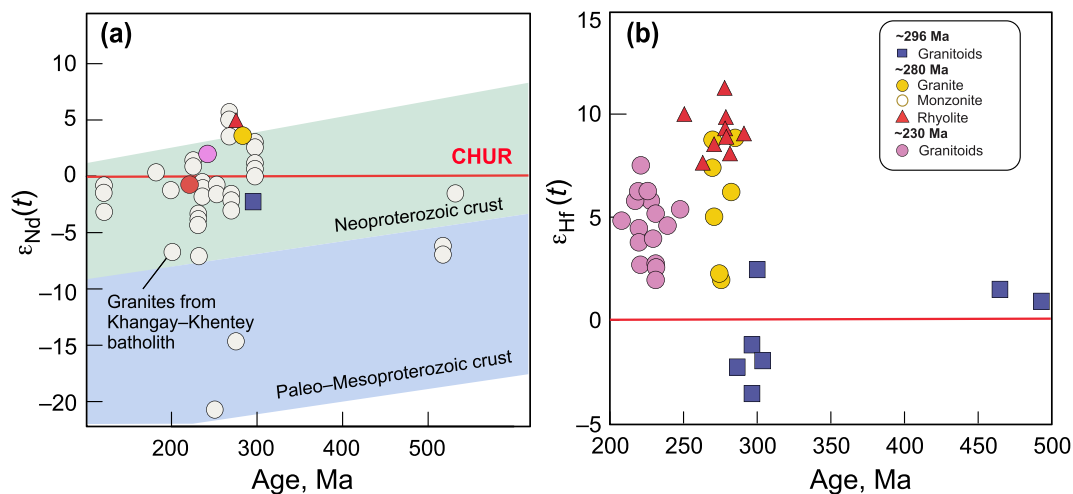


Fig. 9. (a) Correlations between whole-rock $\epsilon_{\text{Nd}}(t)$ and concordia ages; (b) Correlations between $\epsilon_{\text{Hf}}(t)$ and U–Pb ages of zircons for the studied samples from the Khangay-Khentey basin.

central CAOB was very complicated including co-existence of two oceanic basins during this time: (1) Paleo-Asian Ocean to in the south (in present-day coordinates) (e.g., Windley et al., 2007; Xiao et al., 2004), and (2) Mongol-Okhotsk to the north (e.g., Tomurtogoo et al., 2005). We suggest that the emplacement of the ~296 Ma granitoids are likely related to the evolution of the MOO, because the study area is located too far away (>600 km) from the Paleo-Asian suture zone, i.e. the Solonker suture (Badarch et al., 2002; Jian et al., 2012). The study area is also tectonically isolated from the southern domain by the Main Mongolian Lineament and the Central Mongolia-Erguna continental block (Fig. 1c).

The late Carboniferous to early Permian A-type granites and highly alkaline igneous rocks are widely distributed south of the Main Mongolian Lineament (South Mongolia and Inner Mongolia). Studies proposed a “Central Asian Rift System” as responsible for the emplacement of abundant A-type granitic batholiths (Kovalenko et al., 2004; Yarmolyuk et al., 2014). This rift system is linked to a hot-spot or locally, perhaps, the Tarim Large Igneous Province (LIP). However, unlike the

Tarim LIP or other areas of the “Central Asian Rift System”, the study area lacks alkaline basalt, comendite, pantellerite, or nepheline syenite and A₁-type granitoids, and related OIB-basalts which are considered as a result of a mantle plume. Therefore, we think that the ~280 Ma igneous rocks were emplaced in a setting of weak local extension rather than in relation to a plume-induced rifting. By analogy with the ~296 Ma granitoids, we consider that the ~280 Ma magmatism was unlikely related to the evolution of the Paleo-Asian Ocean. We support that the subduction of the MOO formed the Late Paleozoic to Early Mesozoic granitoids and associated volcanics in the magmatic fields outcropped in the Khangay-Khentey region (Fig. 1c) (e.g., Donskaya et al., 2013; Zhao et al., 2017). The northward subduction of the MOO lithosphere beneath the Siberian Craton (including its accreted southern margin) has been well-defined, as indicated by the subduction-related Angara-Vitim granitoids and the Permian–Triassic Selenge volcano-plutonic Belt (e.g., Donskaya et al., 2013; Kovach et al., 2012). These magmatic belts were emplaced in several episodes during a period from the late Carboniferous to the Jurassic. In contrast to the northern part of the Mongol-

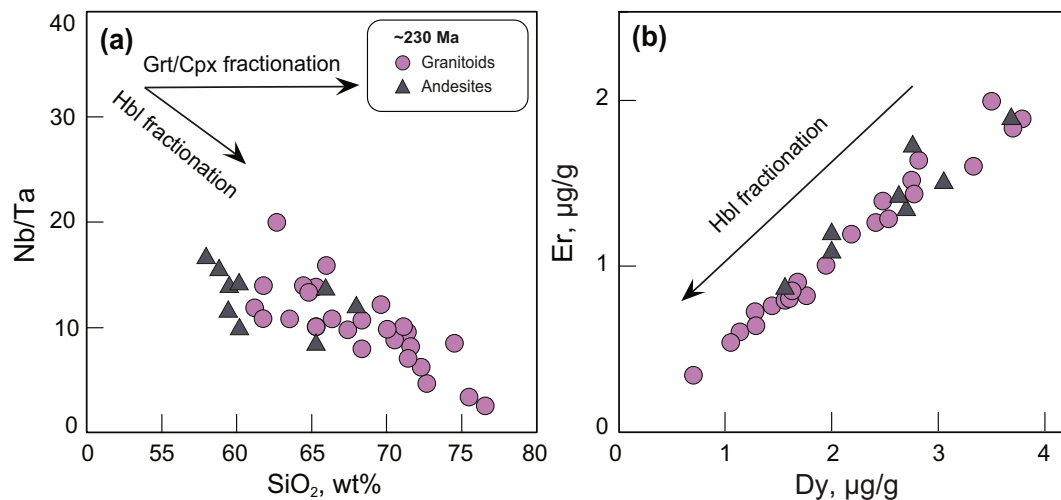


Fig. 10. (a) Nb/Ta versus SiO₂ and (b) Er versus Dy diagrams showing hornblende fractionation for the ~230 Ma rock association from the Khangay-Khenty basin.

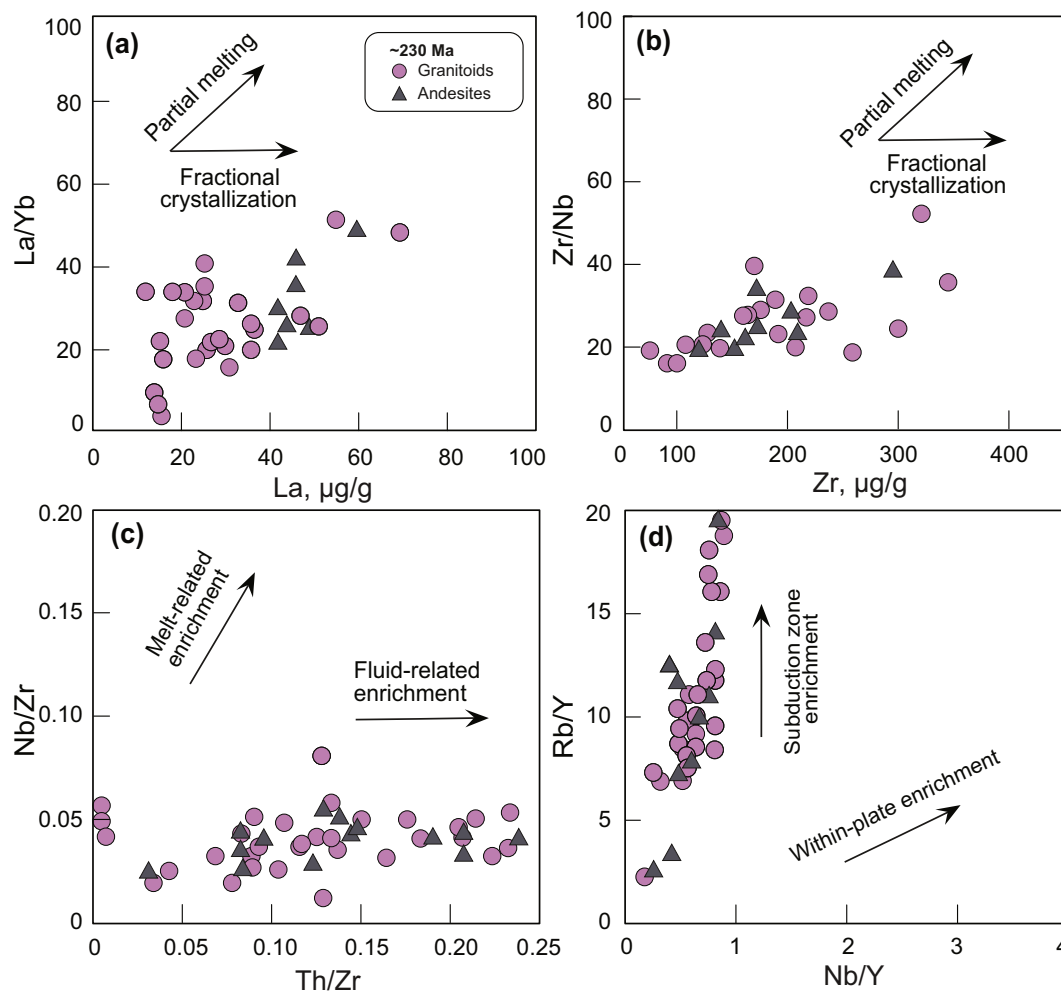


Fig. 11. (a) Plots of La/Yb versus La; (b) Zr/Nb versus Zr; (c) Nb/Zr versus Th/Zr; (d) Rb/Y versus Nb/Y for the ~230 Ma rock associations from the Khangay-Khenty basin.

Okhotsk suture zone, the tectonic evolution of the southern part has been better reconstructed in the Erguna Belt, NE China (Liu et al., 2018; Sun et al., 2013), and to a lesser extent, in the Khangay area (e.g., Dolzodmaa et al., 2020). According to the detrital and igneous rock ages, the southern subduction of the Mongol-Okhotsk oceanic plate started in

the Carboniferous and continued until the early–middle Jurassic (e.g., Bussien et al., 2011; Kelty et al., 2008; Liu et al., 2018). However, the evidence for Late Paleozoic magmatism in the Central Mongolian side was very scarce (Fig. 1c). Our new data provide an important piece to solve the evolution tectonic evolution puzzle of the MOO plate during

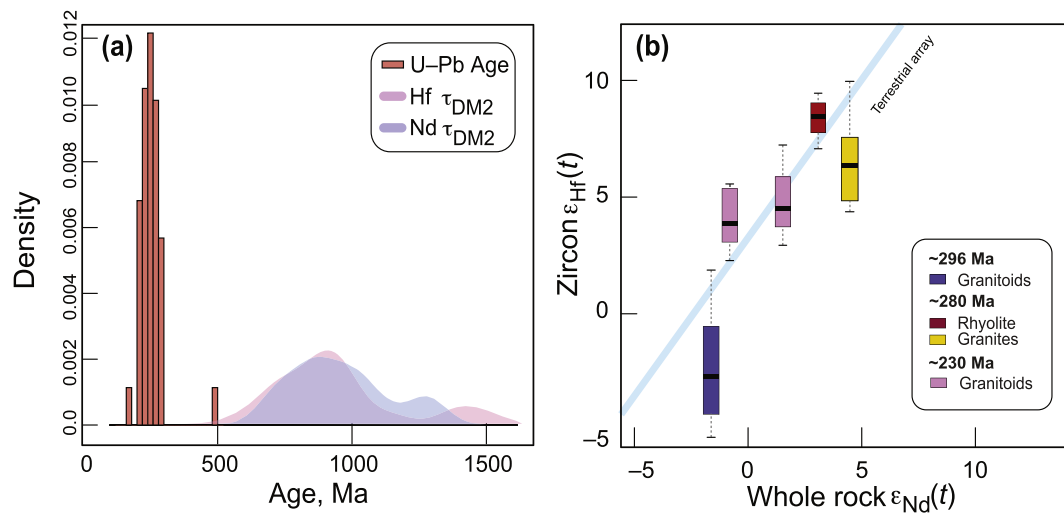


Fig. 12. (a) Histogram shows zircon U–Pb age, two-stage crustal Hf, and Nd model ages; (b) Plots of whole-rock $\epsilon_{Nd}(t)$ versus zircon $\epsilon_{Hf}(t)$ of the studied samples from the Khangay-Khentei basin. The terrestrial array is from [Vervoort et al. \(1999\)](#).

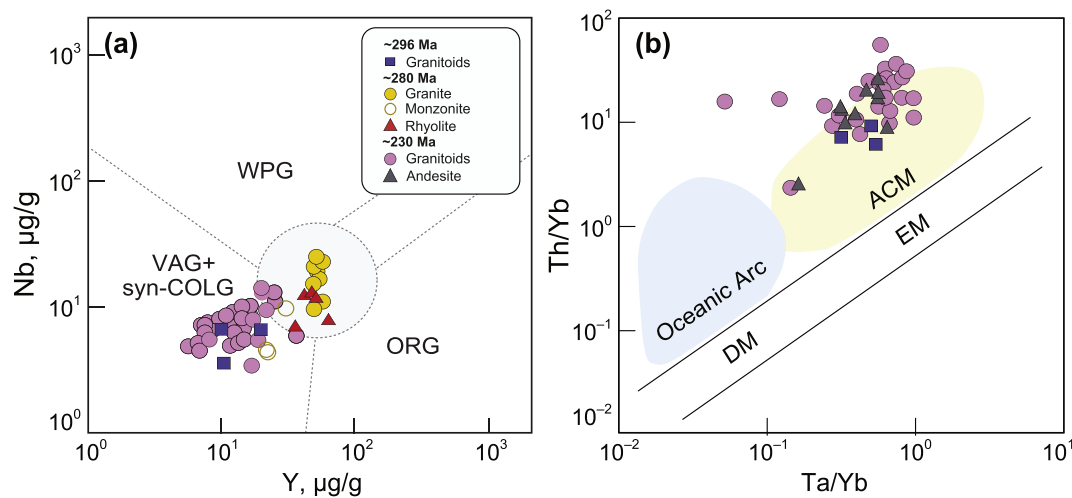


Fig. 13. Tectonic discrimination diagrams for the studied samples from the Khangay-Khentei basin in Central Mongolia: (a) Nb versus Y ([Pearce et al., 1984](#)); (b) Th/Yb versus Ta/Yb (after [Pearce, 1983](#)). Syn-COLG–syn-collision granite; VAG–volcanic arc granite, WPG–within plate granite, Post-COLG–post-collisional granite; ACM–active continental margin; DM–depleted mantle; EM–Enriched mantle.

the Late Paleozoic in Central Mongolia. The U–Pb ages, geochemical, and isotope data from the ~230 Ma granitoids agree with the previous data and indicate emplacement of magmatic rocks in early Permian–late Triassic time. In addition, there is no systematic WE younging of magmatic ages in the southern segment of the Mongol-Okhotsk Belt ([Fig. 1c](#)). Consequently, the ~230 Ma rocks probably formed during the southward subduction of the MOO lithosphere in a tectonic setting of an Andean-type active continental margin. Our new data support the idea of the subduction of the MOO plate beneath the Central Mongolia-Erguna Block during the early Permian–Late Triassic from the Mongolian side.

6. Conclusions

Our new U–Pb zircon ages, whole-rock geochemical data, and in situ Hf-in-zircon and whole-rock Sm–Nd isotope characteristics obtained from Late Paleozoic–Early Mesozoic granitoids of Khangay-Khentei basin in Central Mongolia allowed us to conclude the following.

- (1) The Late Paleozoic–Early Mesozoic granitic rocks in the Khangay-Khentei basin formed at three different times, which were

emplaced in early Permian (~296 Ma), Permian (~280 Ma), and middle Triassic (~230 Ma), respectively.

- (2) The ~296 Ma granitoids include I-type quartz monzonite and granodiorites derived from crustal (recycled) and mantle (mixed or juvenile) sources and their Cambrian age is superseded.
- (3) The ~280 Ma volcanic and plutonic rocks are A_2 -type granites, monzonites, and rhyolites. Monzonites were derived from a mafic source, whereas granites and rhyolites were derived from a source containing Neoproterozoic crustal materials and depleted mantle material. The ~280 Ma rocks were emplaced in a local extension environment linked with magmatic underplating and/or asthenosphere upwelling.
- (4) The ~230 Ma group includes I-type granitoids and volcanic rocks. They were generated from partial melting of a juvenile lower crustal source with the contribution of ancient crust. They formed at an Andean-type active continental margin related to the southward subduction of the Mongol-Okhotsk Ocean beneath the Central Mongolia-Erguna Block.

Supplementary data to this article can be found online at <https://doi.org/10.1016/j.lithos.2021.106455>.

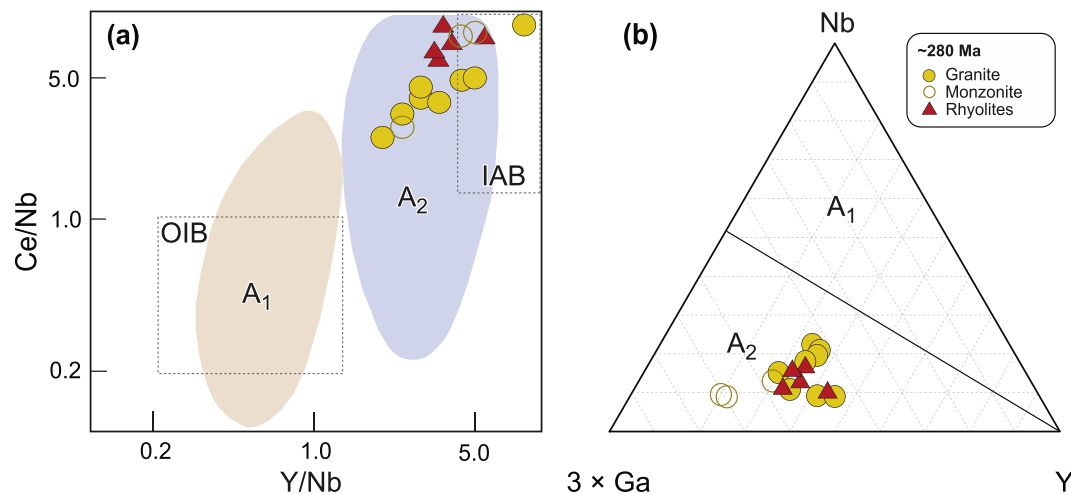


Fig. 14. (a) Ce/Nb versus Y/Nb and (b) $3 \times \text{Ga}$ –Nb–Y subdivision diagrams (after Eby, 1992) for A-type granites for the ~280 Ma rock association from the Khangay-Khentei basin. A₁–continental rift or intra-plate magmatism-related granite; A₂– post-collisional setting or island-arc related granite. IAB–island arc basalt; OIB–oceanic island basalt.

Declaration of Competing Interest

The authors declare that they have no known competing financial interests or personal relationships that could have appeared to influence the work reported in this paper.

Acknowledgments

This research was supported by CNEAS and FRIS of Tohoku University and in part by grants from the MEXT/JSPS KAKENHI JP18H01299 and JP21H01174 to TT and JP19K04043 to KA, by the National Natural Science Foundation of China (grant number 41772230) to L. Miao, and by the Russian Science Foundation (grants #20-77-10051 to Ilya S., Nd isotopes, and #21-77-20022 to Inna S., tectonic implications). AG gratefully acknowledges the Japanese Government MEXT Scholarship. We also thank Isamu Morita, and Manzshir Bayarbold, Sanchir Dorjgochoo for their assistance in the laboratory and for providing geological material. We are grateful for the constructive reviews of V. Kovach, Xian-Hua Li, and an anonymous reviewer, which all helped us to improve the manuscript. Contribution to IGCP#662.

References

- Amar-Amgalan, S., 2008. U-Pb Geochronology and Multi-Isotopic Systematics of Granitoids from Mongolia, Central Asian Orogenic Belt: Implications for Granitoid Origin and Crustal Growth during the Phanerozoic. Unpublished Ph.D. Thesis. Okayama University, Japan, p. 162.
- Aoki, S., Aoki, K., Tsujimori, T., Sakata, S., Tsuchiya, Y., 2020. Oceanic-arc subduction, stagnation, and exhumation: zircon U-Pb geochronology and trace-element geochemistry of the Sanbagawa eclogites in Central Shikoku, SW Japan. *Lithos* 358, 105378. <https://doi.org/10.1016/j.lithos.2020.105378>.
- Badarch, G., Cunningham, W.D., Windley, B.F., 2002. A new terrane subdivision for Mongolia: implications for the Phanerozoic crustal growth of Central Asia. *J. Asian Earth Sci.* 21, 87–110. [https://doi.org/10.1016/S1367-9120\(02\)00017-2](https://doi.org/10.1016/S1367-9120(02)00017-2).
- Barnes, C.G., Ernst, W.G., Berry, R., Tsujimori, T., 2016. Petrology and geochemistry of an upper crustal pluton: a view into crustal-scale magmatism during arc to retro-arc transition. *J. Petrol.* 57 (7), 1361–1388. <https://doi.org/10.1093/petrology/egw043>.
- Black, L.P., Kamo, S.L., Allen, C.M., Aleinikoff, J.N., Davis, D.W., Korsch, R.J., Foudoulis, C., 2003. TEMORA 1: a new zircon standard for Phanerozoic U-Pb geochronology. *Chem. Geol.* 200, 155–170. [https://doi.org/10.1016/S0009-2541\(03\)00165-7](https://doi.org/10.1016/S0009-2541(03)00165-7).
- Bonin, B., 2007. A-type granites and related rocks: evolution of a concept, problems and prospects. *Lithos* 97, 1–29. <https://doi.org/10.1016/j.lithos.2006.12.007>.
- Bouvier, A., Vervoort, J.D., Patchett, P.J., 2008. The Lu-Hf and Sm-Nd isotopic composition of CHUR: constraints from unequilibrated chondrites and implications for the bulk composition of terrestrial planets. *Earth Planet. Sci. Lett.* 273, 48–57.
- Bussien, D., Gombojav, N., Winkler, W., Von Quadt, A., 2011. The Mongol-Okhotsk Belt in Mongolia—an appraisal of the geodynamic development by the study of

- sandstone provenance and detrital zircons. *Tectonophysics* 510, 132–150. <https://doi.org/10.1016/j.tecto.2011.06.024>.
- Chappell, B.W., Bryant, C.J., Wyborn, D., 2012. Peraluminous I-type granites. *Lithos* 153, 142–153. <https://doi.org/10.1016/j.lithos.2012.07.008>.
- Chen, G.N., Grapes, R., 2007. *Granite Genesis: In-Situ Melting and Crustal Evolution*, first ed. Springer, Dordrecht, Netherlands.
- Chu, Z.Y., Wu, F.Y., Walker, R.J., Rudnick, R.L., Pitcher, L., Puchtel, I.S., Yang, Y.H., Wilde, S.A., 2009. Temporal evolution of the lithospheric mantle beneath the eastern North China Craton. *J. Petrol.* 50 (10), 1857–1898.
- Clemens, J.D., Stevens, G., Bryan, S.E., 2020. Conditions during the formation of granitic magmas by crustal melting—hot or cold; drenched, damp or dry? *Earth Sci. Rev.* 200, 102982.
- Collins, W.J., Huang, H.Q., Bowden, P., Kemp, A.I.S., 2020. Repeated S–I–A-type granite trilogy in the Lachlan Orogen and geochemical contrasts with A-type granites in Nigeria: implications for petrogenesis and tectonic discrimination. *Geol. Soc. Lond., Spec. Publ.* 491, 53–76. <https://doi.org/10.1144/SP491-2018-159>.
- Dagvadorj, D., Bold, G., Chuluun, D., Gundsambuu, Ts., 1993. *Geological Map of the Central and Eastern Mongolia*, Scale 1:500,000. Institute of Geological Research Regional Geological Sector, Ministry of Heavy industrial (in Mongolian).
- Dagva-Ochir, L., Oyunchimeg, T.U., Enkhdalai, B., Safonova, L., Li, H., Otgonbaatar, D., Tamehe, L.S., Sharav, D., 2020. Middle Paleozoic intermediate-mafic rocks of the Tsoroidog Uul accretionary complex, Central Mongolia: Petrogenesis and tectonic implications. *Lithos* 376, 105795. <https://doi.org/10.1016/j.lithos.2020.105795>.
- Dahlquist, J.A., Alasino, P.H., Eby, G.N., Galindo, C., Casquet, C., 2010. Fault controlled Carboniferous A-type magmatism in the proto-Andean foreland (Sierras Pampeanas, Argentina): Geochemical constraints and petrogenesis. *Lithos* 115, 65–81.
- Dolzodmaa, B., Osanai, Y., Nakano, N., Adachi, T., 2020. Zircon U-Pb geochronology and geochemistry of granitic rocks in Central Mongolia. *Mongolian Geosci.* 50, 23–44. <https://doi.org/10.5564/mgs.v50i0.1327>.
- Donskaya, T.V., Gladkochub, D.P., Mazukabzov, A.M., Ivanov, A.V., 2013. Late Paleozoic–Mesozoic subduction-related magmatism at the southern margin of the Siberian continent and the 150 million-year history of the Mongol-Okhotsk Ocean. *J. Asian Earth Sci.* 62, 79–97. <https://doi.org/10.1016/j.jseaes.2012.07.023>.
- Eby, G.N., 1992. Chemical subdivision of the A-type granitoids: petrogenetic and tectonic implications. *Geology* 20, 641–644.
- Ehiro, M., Zakharov, Y.U., Minjini, C., 2006. Early Triassic (Olenekian) ammonoids from Khentey Province, Mongolia, and their paleobiogeographic significance. *Bull. Tohoku Univ. Museum* 83–97.
- Frost, B.R., Barnes, C.G., Collins, W.J., Arculus, R.J., Ellis, D.J., Frost, C.D., 2001. A geochemical classification for granitic rocks. *J. Petrol.* 42, 2033–2048.
- Ganbat, A., Tsujimori, T., Boniface, N., Pastor-Galán, D., Aoki, S., Aoki, K., 2021a. Crustal evolution of the Paleoproterozoic Ubendian Belt (SW Tanzania) western margin: a central African Shield amalgamation tale. *Gondwana Res.* 91, 286–306. <https://doi.org/10.1016/j.gr.2020.12.009>.
- Ganbat, A., Pastor-Galán, D., Hirano, N., Nakamura, N., Sumino, H., Yamaguchi, Y., Tsujimori, T., 2021b. Cretaceous to Miocene NW Pacific Plate kinematic constraints: Paleomagnetism and Ar-Ar geochronology in the Mineoka Ophiolite Mélange (Japan). *Journal of Geophysical Research: Solid Earth* v. 126. <https://doi.org/10.1029/2020JB021492> e2020JB021492.
- Goldstedt, S.J., Jacobsen, S.B., 1988. Nd and Sr isotopic systematics of river water suspended material: implications for crustal evolution. *Earth Planet. Sci. Lett.* 87, 249–265.
- Grebennikov, A.V., Khanchuk, A.I., Gonevchuk, V.G., Kovalenko, S.V., 2016. Cretaceous and Paleogene granitoid suites of the Sikhote-Alin area (Far East Russia): Geochemistry and tectonic implications. *Lithos* 261, 250–261. <https://doi.org/10.1016/j.lithos.2015.12.020>.

- Green, T.H., 1995. Significance of Nb/Ta as an indicator of geochemical processes in the crust-mantle system. *Chem. Geol.* 120, 347–359.
- Griffin, W.L., Belousova, E.A., Shee, S.R., Pearson, N.J., O'Reilly, S.Y., 2004. Archean crustal evolution in the northern Yilgarn Craton: U–Pb and Hf-isotope evidence from detrital zircons. *Precambrian Res.* 131, 231–282. <https://doi.org/10.1016/j.precamres.2003.12.011>.
- Hara, H., Kurihara, T., Tsukada, K., Kon, Y., Uchino, T., Suzuki, T., Takeuchi, M., Nakane, Y., Nuramkhan, M., Chuluun, M., 2013. Provenance and origins of a late Paleozoic accretionary complex within the Khangai–Khentei belt in the Central Asian Orogenic Belt, Central Mongolia. *J. Asian Earth Sci.* 75, 141–157. <https://doi.org/10.1016/j.jseas.2013.06.006>.
- Harada, H., Tsujimori, T., Kunugiza, K., Yamashita, K., Aoki, S., Aoki, K., Takayanagi, H., Iryu, Y., 2021. The $\delta^{13}\text{C}$ – $\delta^{18}\text{O}$ variations in marble in the Hida Belt, Japan. *Island Arc* 40, e12389. <https://doi.org/10.1111/iar.12389>.
- Hoffmann, J.E., Münker, C., Polat, A., Rosing, M.T., Schulz, T., 2011. The origin of decoupled Hf–Nd isotope compositions in Earth's earliest rocks from southern West Greenland. *Geochim. Cosmochim. Acta* 75, 6610–6628. <https://doi.org/10.1016/j.gca.2011.08.018>.
- Irvine, T.N., Baragar, W.R.A., 1971. A guide to the chemical classification of the common volcanic rocks. *Can. J. Earth Sci.* 8, 523–548.
- Jacobsen, S.B., Wasserburg, G.J., 1984. Sm–Nd isotopic evolution of chondrites and achondrites, II. *Earth Planet. Sci. Lett.* 67, 137–150. [https://doi.org/10.1016/0012-821X\(84\)90109-2](https://doi.org/10.1016/0012-821X(84)90109-2).
- Jahn, B.M., 2004. The Central Asian Orogenic Belt and growth of the continental crust in the Phanerozoic. *Geol. Soc. Lond., Spec. Publ.* 226, 73–100.
- Jian, P., Kröner, A., Windley, B.F., Shi, Y., Zhang, W., Zhang, L., Yang, W., 2012. Carboniferous and cretaceous mafic–ultramafic massifs in Inner Mongolia (China): a SHRIMP zircon and geochemical study of the previously presumed integral “Hegenshan ophiolite”. *Lithos* 142, 48–66. <https://doi.org/10.1016/j.lithos.2012.03.007>.
- Jochum, K.P., Weis, U., Stoll, B., Kuzmin, D., Yang, Q., Raczek, I., Jacob, D.E., Stracke, A., Birbaum, K., Frick, D.A., Günther, D., 2011. Determination of reference values for NIST SRM 610–617 glasses following ISO guidelines. *Geostand. Geoanal. Res.* 35, 397–429. <https://doi.org/10.1111/j.1751-908X.2011.00120.x>.
- Jones, M.R., Soule, S.A., Gonnermann, H.M., Le Roux, V., Clague, D.A., 2018. Magma ascent and lava flow emplacement rates during the 2011 Axial Seamount eruption based on CO_2 degassing. *Earth Planet. Sci. Lett.* 494, 32–41. <https://doi.org/10.1016/j.epsl.2018.04.044>.
- Kelty, T.K., Yin, A., Dash, B., Gehrels, G.E., Ribeiro, A.E., 2008. Detrital-zircon geochronology of Paleozoic sedimentary rocks in the Hangay–Hentey basin, north-Central Mongolia: implications for the tectonic evolution of the Mongol–Okhotsk Ocean in Central Asia. *Tectonophysics* 451, 290–311. <https://doi.org/10.1016/j.tecto.2007.11.052>.
- Kemp, A.I.S., Hawkesworth, C.J., Paterson, B.A., Kinny, P.D., 2006. Episodic growth of the Gondwana supercontinent from hafnium and oxygen isotopes in zircon. *Nature* 439, 580–583.
- Kemp, A.I.S., Hawkesworth, C.J., Foster, G.L., Paterson, B.A., Woodhead, J.D., Hergt, J.M., Gray, C.M., Whitehouse, M.J., 2007. Magmatic and crustal differentiation history of granitic rocks from Hf–O isotopes in zircon. *Science* 315, 980–983.
- Kovach, V.P., Sal'nikova, E.B., Ryt'sk, E.Yu., Yarmolyuk, V.V., Kotov, A.B., Anisimova, I.V., Yakovleva, S.Z., Fedoseenko, A.M., Plotkina, Yu.V., 2012. The time length of formation of the Angara–Vitim Batholith: results of U–Pb geochronological studies. *Dokl. Earth Sci.* 444, 553–558.
- Kovalenko, V.I., Yarmolyuk, V.V., Kovach, V.P., Kotov, A.B., Kozakov, I.K., Salnikova, E.B., 1996. Sources of Phanerozoic granitoids in Central Asia: Sm–Nd isotope data. *Geochem. Int.* 34, 628–640.
- Kovalenko, V.I., Yarmolyuk, V.V., Kovach, V.P., Kotov, A.B., Kozakov, I.K., Salnikova, E.B., Larin, A.M., 2004. Isotope provinces, mechanism of generation and sources of the continental crust in the Central Asian Mobile Belt: geological and isotopic evidence. *J. Asian Earth Sci.* 23, 605–627.
- Kozakov, I.K., Kovach, V.P., Bibikova, E.V., Kirnozova, T.I., Zagornaya, N.Y., Plotkina, Y.V., Podkovyrov, V.N., 2007. Age and sources of granitoids in the junction zone of the Caledonides and Hercynides in southwestern Mongolia: geodynamic implications. *Petrology* 15, 126–150.
- Kröner, A., Kovach, V., Belousova, E., Hegner, E., Armstrong, R., Dolgoplova, A., Seltmann, R., Alexeiev, D.V., Hoffmann, J.E., Wong, J., Sun, M., 2014. Reassessment of continental growth during the accretionary history of the Central Asian Orogenic Belt. *Gondwana Res.* 25, 103–125. <https://doi.org/10.1016/j.gr.2012.12.023>.
- Lamb, M.A., Badarch, G., Hendrix, M.S., Davis, G.A., 2001. Paleozoic sedimentary basins and volcanic arc systems of southern Mongolia: new geochemical and petrographic constraints. *Memoirs-Geol. Soc. Am.* 117–150.
- Le Bas, M., Maitre, R.L., Streckeis, A., Zanettin, B., 1986. A chemical classification of volcanic rocks based on the total alkali-silica diagram. *J. Petrol.* 27, 745–750.
- Litvinovsky, B.A., Tsygankov, A.A., Jahn, B.M., Katzir, Y., Be'eri-Shelevin, Y., 2011. Origin and evolution of overlapping calc-alkaline and alkaline magmas: the late Palaeozoic post-collisional igneous province of Transbaikalia (Russia). *Lithos* 125, 845–874. <https://doi.org/10.1016/j.lithos.2011.04.007>.
- Liu, H., Li, Y., He, H., Huangfu, P., Liu, Y., 2018. Two-phase southward subduction of the Mongol–Okhotsk oceanic plate constrained by Permian–Jurassic granitoids in the Erguna and Xing'an massifs (NE China). *Lithos* 304, 347–361. <https://doi.org/10.1016/j.lithos.2018.01.016>.
- Macpherson, C.G., Dreher, S.T., Thirlwall, M.F., 2006. Adakites without slab melting: high pressure differentiation of island arc magma, Mindanao, the Philippines. *Earth Planet. Sci. Lett.* 243, 581–593. <https://doi.org/10.1016/j.epsl.2005.12.034>.
- Maniar, P.D., Piccoli, P.M., 1989. Tectonic discrimination of granitoids. *Geol. Soc. Am. Bull.* 101, 635–643.
- Maruyama, S., Seno, T., 1986. Orogeny and relative plate motions: Example of the Japanese Islands. *Tectonophysics* 127, 305–329. [https://doi.org/10.1016/0040-1951\(86\)90067-3](https://doi.org/10.1016/0040-1951(86)90067-3).
- Morel, M.L.A., Nebel, O., Nebel-Jacobsen, Y.J., Miller, J.S., Vroon, P.Z., 2008. Hafnium isotope characterization of the GJ-1 zircon reference material by solution and laser-ablation MC-ICPMS. *Chem. Geol.* 255, 231–235. <https://doi.org/10.1016/j.chemgeo.2008.06.040>.
- Morozumi, H., 2003. Geochemical characteristics of granitoids of the Erdenet porphyry copper deposit, Mongolia. *Resour. Geol.* 53, 311–316. <https://doi.org/10.1111/j.1751-3928.2003.tb00180.x>.
- Moyen, J.F., 2009. High Sr/Y and La/Yb ratios: the meaning of the “adakitic signature”. *Lithos* 112, 556–574.
- Munktsengel, B., Ohara, M., Gerel, O., Dandar, S., Tsuchiya, N., 2007. Preliminary study of formation mechanism of the erdenetiin ovoo porphyry copper-molybdenum deposit and environmental effects of Erdenet Mine, Northern Mongolia. In: *AIP Conference Proceedings*, 833, 204–207. Physics, American Institute of. <https://doi.org/10.1063/1.2207106>.
- Pastor-Galán, D., Spencer, C.J., Furukawa, T., Tsujimori, T., 2021. Evidence for crustal removal, tectonic erosion and flare-ups from the Japanese evolving forearc sediment provenance. *Earth Planet. Sci. Lett.* 564, 116893. <https://doi.org/10.1016/j.epsl.2021.116893>.
- Patiño Douce, A.E., 1997. Generation of metaluminous A-type granites by low-pressure melting of calc-alkaline granitoids. *Geology* 25, 743–746.
- Pearce, J.A., 1983. The role of sub-continental lithosphere in magma genesis at destructive plate margins. *Continental Basalts and Mantle Xenoliths*. Shiva Publishing, Nantwich, Cheshire, pp. 230–249.
- Pearce, J.A., Peate, D.W., 1995. Tectonic implications of the composition of volcanic arc magmas. *Annu. Rev. Earth Planet. Sci.* 23, 251–286.
- Pearce, J.A., Harris, N.B., Tindle, A.G., 1984. Trace element discrimination diagrams for the tectonic interpretation of granitic rocks. *J. Petrol.* 25, 956–983.
- Peccerillo, A., Taylor, S.R., 1976. Geochemistry of Eocene calc-alkaline volcanic rocks from the Kastamonu area, northern Turkey. *Contrib. Mineral. Petrol.* 58, 63–81.
- Rudnick, R.L., Gao, S., 2003. Composition of the continental crust. In: Gao, S., Holland, H.D., Turekian, K.K. (Eds.), *The Crust*, 3. Elsevier, Amsterdam, Netherlands, pp. 1–64.
- Ruppen, D., Knaf, A., Bussien, D., Winkler, W., Chimedtseren, A., von Quadt, A., 2014. Restoring the Silurian to Carboniferous northern active continental margin of the Mongol–Okhotsk Ocean in Mongolia: Hangay–Hentey accretionary wedge and seamount collision. *Gondwana Res.* 25, 1517–1534. <https://doi.org/10.1016/j.gr.2013.05.022>.
- Safonova, I., 2017. Juvenile versus recycled crust in the Central Asian Orogenic Belt: Implications from ocean plate stratigraphy, blueschist belts and intra-oceanic arcs. *Gondwana Res.* 47, 6–27.
- Safonova, I., Seltmann, R., Kröner, A., Gladkochub, D., Schulmann, K., Xiao, W., Kim, J., Komiya, T., Sun, M., 2011. A new concept of continental construction in the Central Asian Orogenic Belt. *Episodes* 34, 186–196.
- Safonova, I., Kotlyarov, A., Krivonogov, S., Xiao, W., 2017. Intra-oceanic arcs of the Paleo-Asian Ocean. *Gondwana Res.* 50, 167–194.
- Şengör, A.M.C., Natal'in, B.A., Burtman, V.S., 1993. Evolution of the Altai tectonic collage and Paleozoic crustal growth in Eurasia. *Nature* 364, 299–307.
- Sláma, J., Košler, J., Condon, D.J., Crowley, J.L., Gerdes, A., Hancher, J.M., Horstwood, M.S., Morris, G.A., Nasdala, L., Norberg, N., Schaltegger, U., 2008. Pleisovca zircon—a new natural reference material for U–Pb and Hf isotopic microanalysis. *Chem. Geol.* 249, 1–35. <https://doi.org/10.1016/j.chemgeo.2007.11.005>.
- Söderlund, U., Patchett, P.J., Vervoort, J.D., Isachsen, C.E., 2004. The ^{176}Lu decay constant determined by Lu–Hf and U–Pb isotope systematics of Precambrian mafic intrusions. *Earth Planet. Sci. Lett.* 219, 311–324. [https://doi.org/10.1016/S0012-821X\(04\)00012-3](https://doi.org/10.1016/S0012-821X(04)00012-3).
- Sorokin, A.A., Zaika, V.A., Kovach, V.P., Kotov, A.B., Xu, W., Yang, H., 2020. Timing of closure of the eastern Mongol–Okhotsk Ocean: Constraints from U–Pb and Hf isotopic data of detrital zircons from metasediments along the Dzhangdy Transect. *Gondwana Res.* 81, 58–78. <https://doi.org/10.1016/j.gr.2019.11.009>.
- Sun, S.S., McDonough, W.F., 1989. Chemical and isotopic systematics of oceanic basalts: implications for mantle composition and processes. *Geol. Soc. Lond., Spec. Publ.* 42, 313–345. <https://doi.org/10.1144/GSL.SP.1989.042.01.19>.
- Sun, D.Y., Gou, J., Wang, T.H., Ren, Y.S., Liu, Y.J., Guo, H.Y., Liu, X.M., Hu, Z.C., 2013. Geochronological and geochemical constraints on the Erguna massif basement, NE China—subduction history of the Mongol–Okhotsk oceanic crust. *Int. Geol. Rev.* 55, 1801–1816.
- Taylor, S.R., McLennan, S.M., 1995. The geochemical evolution of the continental crust. *Rev. Geophys.* 33, 241–265.
- Tiepolo, M., Vannucci, R., 2014. The contribution of amphibole from deep arc crust to the silicate Earth's Nb budget. *Lithos* 208, 16–20. <https://doi.org/10.1016/j.lithos.2014.07.028>.
- Tiepolo, M., Oberti, R., Zanetti, A., Vannucci, R., Foley, S.F., 2007. Trace-element partitioning between amphibole and silicate melt. *Rev. Mineral. Geochem.* 67, 417–452.
- Tomurtogoo, O., Windley, B.F., Kröner, A., Badarch, G., Liu, D.Y., 2005. Zircon age and occurrence of the Adaatsag ophiolite and Muroon shear zone, Central Mongolia: constraints on the evolution of the Mongol–Okhotsk Ocean, suture and orogen. *J. Geol. Soc.* 162, 125–134. <https://doi.org/10.1144/0016-764903-146>.
- Tumurchudor, D., Bold, G., Chuluun, D., Gundsambuu, Ts., 2006. Geological Map of the Ikh-Khungeba Area, Scale 1:50,000. GURVANTAL LLC, Mongolia (in Mongolian).

- Turner, S.P., Foden, J.D., Morrison, R.S., 1992. Derivation of some A-type magmas by fractionation of basaltic magma: an example from the Padthaway Ridge, South Australia. *Lithos* 28, 151–179. [https://doi.org/10.1016/0024-4937\(92\)90029-X](https://doi.org/10.1016/0024-4937(92)90029-X).
- Vermeesch, P., 2018. IsoplotR: a free and open toolbox for geochronology. *Geosci. Front.* 9 (5), 1479–1493. <https://doi.org/10.1016/j.gsf.2018.04.001>.
- Vervoort, J.D., Patchett, P.J., Blichert-Toft, J., Albarède, F., 1999. Relationships between Lu-Hf and Sm-Nd isotopic systems in the global sedimentary system. *Earth Planet. Sci. Lett.* 168, 79–99.
- Whalen, J.B., Currie, K.L., Chappell, B.W., 1987. A-type granites: geochemical characteristics, discrimination and petrogenesis. *Contrib. Mineral. Petrol.* 95, 407–419.
- Wiedenbeck, M., Hanchar, J.M., Peck, W.H., Sylvester, P., Valley, J., Whitehouse, M., Kronz, A., Morishita, Y., Nasdala, L., Fiebig, J., Franchi, I., 2004. Further characterisation of the 91500 zircon crystal. *Geostand. Geoanal. Res.* 28, 9–39.
- Wilhem, C., Windley, B.F., Stampfli, G.M., 2012. The Altaids of Central Asia: a tectonic and evolutionary innovative review. *Earth Sci. Rev.* 113, 303–341. <https://doi.org/10.1016/j.earscirev.2012.04.001>.
- Windley, B.F., Alexeiev, D., Xiao, W., Kröner, A., Badarch, G., 2007. Tectonic models for accretion of the Central Asian Orogenic Belt. *J. Geol. Soc.* 164, 31–47. <https://doi.org/10.1144/0016-76492006-022>.
- Xiao, W.J., Zhang, L.C., Qin, K.Z., Sun, S.H.U., Li, J.L., 2004. Paleozoic accretionary and collisional tectonics of the Eastern Tianshan (China): implications for the continental growth of Central Asia. *Am. J. Sci.* 304, 370–395.
- Xiao, W., Huang, B., Han, C., Sun, S., Li, J., 2010. A review of the western part of the Altaids: a key to understanding the architecture of accretionary orogens. *Gondwana Res.* 18, 253–273.
- Yarmolyuk, V.V., Kovalenko, V.I., Sal'nikova, E.B., Budnikov, S.V., Kovach, V.P., Kotov, A.B., Ponomarchuk, V.A., 2002. Tectono-magmatic zoning, magma sources, and geodynamics of the Early Mesozoic Mongolia-Transbaikal province. *Geotectonics* 36, 293–311.
- Yarmolyuk, V.V., Kuzmin, M.I., Ernst, R.E., 2014. Intraplate geodynamics and magmatism in the evolution of the Central Asian Orogenic Belt. *J. Asian Earth Sci.* 93, 158–179. <https://doi.org/10.1016/j.jseae.2014.07.004>.
- Yarmolyuk, V.V., Kozlovsky, A.M., Savatenkov, V.M., Kovach, V.P., Kozakov, I.K., Kotov, A.B., Lebedev, V.I., Eenjin, G., 2016. Composition, sources, and geodynamic nature of giant batholiths in Central Asia: evidence from the geochemistry and Nd isotopic characteristics of granitoids in the Khangai zonal magmatic area. *Petrology* 24, 433–461.
- Yarmolyuk, V.V., Kozlovsky, A.M., Travin, A.V., Kirnozova, T.I., Fugzan, M.M., Kozakov, I.K., Plotkina, Y.V., Eenjin, G., Oyunchimeg, T., Sviridova, O.E., 2019. Duration and geodynamic nature of giant central Asian batholiths: geological and geochronological studies of the Khangai batholith. *Stratigr. Geol. Correl.* 27, 73–94.
- Yi, Z., Meert, J.G., 2020. A closure of the Mongol-Okhotsk Ocean by the Middle Jurassic: Reconciliation of paleomagnetic and geological evidence. *Geophys. Res. Lett.* 47 <https://doi.org/10.1029/2020GL088235>.
- Zhao, P., Xu, B., Jahn, B.M., 2017. The Mongol-Okhotsk Ocean subduction-related Permian peraluminous granites in northeastern Mongolia: Constraints from zircon U-Pb ages, whole-rock elemental and Sr-Nd-Hf isotopic compositions. *J. Asian Earth Sci.* 144, 225–242. <https://doi.org/10.1016/j.jseae.2017.03.022>.
- Zhu, M., Zhang, F., Miao, L., Baatar, M., Anaad, C., Yang, S., Li, X., 2016. Geochronology and geochemistry of the Triassic bimodal volcanic rocks and coeval A-type granites of the Olzit area, Middle Mongolia: Implications for the tectonic evolution of Mongol-Okhotsk Ocean. *J. Asian Earth Sci.* 122, 41–57. <https://doi.org/10.1016/j.jseae.2016.03.001>.
- Zhu, M., Zhang, F., Miao, L., Baatar, M., Anaad, C., Yang, S.H., Li, X.B., 2018. The late Carboniferous Khuhu davaa ophiolite in northeastern Mongolia: Implications for the tectonic evolution of the Mongol-Okhotsk Ocean. *Geol. J.* 53, 1263–1278.